© 2019. Published by The Company of Biologists Ltd | Development (2019) 146, dev177881. doi:10.1242/dev.177881

RESEARCH ARTICLE

Three-dimensional live imaging of Atoh1 reveals the dynamics of hair cell induction and organization in the developing cochlea

Tomoko Tateya[1,2,3,*], Susumu Sakamoto[1,3], Fumiyoshi Ishidate[4], Tsuyoshi Hirashima[5], Itaru Imayoshi[6] and Ryoichiro Kageyama[3,4,7,8,*]

ABSTRACT

During cochlear development, hair cells (HCs) and supporting cells differentiate in the prosensory domain to form the organ of Corti, but how one row of inner HCs (IHCs) and three rows of outer HCs (OHCs) are organized is not well understood. Here, we investigated the process of HC induction by monitoring Atoh1 expression in cochlear explants of *Atoh1*-EGFP knock-in mouse embryos and showed that only the cells that express Atoh1 over a certain threshold are selected for HC fate determination. HC induction initially occurs at the medial edge of the prosensory domain to form IHCs and subsequently at the lateral edge to form OHCs, while Hedgehog signaling maintains a space between IHCs and OHCs, leading to formation of the tunnel of Corti. These results reveal dynamic Atoh1 expression in HC fate control and suggest that multi-directional signals regulate OHC induction, thereby organizing the prototype of the organ of Corti.

KEY WORDS: Atoh1, Cochlea, Hair cell, Live imaging, Mouse

INTRODUCTION

The sensory epithelium of the mammalian cochlea, called the organ of Corti, contains mechanosensory hair cells (HCs) and supporting cells (SCs). There are two types of HCs in the organ of Corti: the inner HCs (IHCs) and outer HCs (OHCs). IHCs detect sound and transmit the signal to the brain via the auditory nerve, whereas OHCs perform a signal-amplifying role. One of the most striking features of the organ of Corti is the tunnel of Corti, which is formed by two rows of pillar cells, a specific subtype of SC, and separates OHCs from IHCs. With the exception of monotremes, the mammalian cochlea contains one row of IHCs and generally three rows of OHCs (Ladhams and Pickles, 1996; Manley and Köppl, 1998). The tunnel of Corti and OHCs are the major distinguishing features of the mammalian cochlea and are essential for normal hearing (Wan et al., 2013).

[1]Department of Otolaryngology – Head and Neck Surgery, Kyoto University Graduate School of Medicine, Kyoto 606-8507, Japan. [2]Department of Speech and Hearing Sciences and Disorders, Faculty of Health and Medical Science, Kyoto University of Advanced Science, Kyoto 615-8577, Japan. [3]Department of Biosystems Science, Institute for Frontier Life and Medical Sciences, Kyoto University, Kyoto 606-8507, Japan. [4]Institute for Integrated Cell-Material Sciences (iCeMS), Kyoto University, Kyoto 606-8501, Japan. [5]Department of Pathology and Biology of Diseases, Graduate School of Medicine, Kyoto University, Kyoto 606-8501, Japan. [6]Research Center for Systemic Life Science, Graduate School of Biostudies, Kyoto University, Kyoto 606-8501, Japan. [7]Department of Growth Regulation, Graduate School of Medicine, Kyoto University, Kyoto 606-8501, Japan. [8]Department of Molecular and Cellular Biology, Graduate School of Biostudies, Kyoto University, Kyoto 606-8501, Japan.

*Authors for correspondence (t_tateya@ent.kuhp.kyoto-u.ac.jp; rkageyam@infront.kyoto-u.ac.jp)

T.T., 0000-0002-0342-3688; T.H., 0000-0001-7323-9627; I.I., 0000-0001-9728-481X; R.K., 0000-0002-5985-1120

Received 12 March 2019; Accepted 27 September 2019

The cochlear duct arises as a ventral out-pocketing of the developing otocyst; subsequent HC development is divided into three steps (Kelly and Chen, 2009). The first step is called prosensory specification. The prosensory domain is formed in the dorsal region of the cochlear duct, referred to as the floor, and is populated by prosensory cells that are the common precursors of HCs and SCs. The second step is the exit of prosensory cells from the cell cycle. The third step is the differentiation of prosensory cells to IHCs, OHCs and several subtypes of SCs. Elucidation of this third step is of considerable importance for future development of regenerative strategies to restore the organ of Corti.

The earliest indication of HC differentiation in the prosensory domain of the mouse cochlea can be observed based on morphology between embryonic day (E) 14 and E15, at which time IHCs differentiate in the mid-basal region, approximately a quarter of the entire cochlear length from the base (Rubel, 1978; Kelley, 2007). IHC differentiation then proceeds in a gradient that extends mainly towards the apex, and slightly toward the base, of the cochlear spiral (Rubel, 1978). There is also a second gradient along the medial-lateral axis of the cochlea from IHCs to OHCs; that is, IHCs differentiate earlier than OHCs (Chen et al., 2002; Kelly and Chen, 2009). The order of subsequent cellular differentiation within the organ of Corti, including that of OHCs and several subtypes of SCs, remains unclear (Kelley, 2007). Developing OHCs can be observed by E15 to E16, but developing SCs, in particular pillar cells, become morphologically distinct around the same time, making it difficult to determine which cells arise first (Kelley, 2007). At the first appearance of OHCs, a space is present between the IHCs and OHCs; the pillar cells arise in this space and the tunnel of Corti is then formed. At this developmental stage, OHCs and IHCs are morphologically similar and can only be identified in relation to the space.

Atoh1, which encodes a proneural bHLH transcription factor, is one of the earliest known genes to be expressed in the prosensory domain and its expression is eventually associated with HCs. The general consensus is that *Atoh1* is one of the first genes expressed in differentiating HCs and is both necessary and sufficient for their differentiation (Bermingham et al., 1999; Zheng and Gao, 2000; Woods et al., 2004). *Atoh1* expression is initially detected as a gradient that is strongest near the cochlear base and, over time, extends towards the apex (Anniko, 1983; Lanford et al., 2000). The timing and pattern of changes in *Atoh1* expression are controversial and there appears to be a difference between the results obtained by using knock-in mice (*Atoh1*$^{+/lacZ}$ mouse and *Atoh1*-EGFP mouse) and an *Atoh1* transgenic reporter mouse (Lumpkin et al., 2003; Cai et al., 2013; Rose et al., 2009). Data generated using *Atoh1*-EGFP mice, in which the endogenous Atoh1 is tagged with EGFP (Rose et al., 2009), appear to be the most sensitive and, therefore, are most reliable for examining the timing and pattern of changes to Atoh1 protein levels (Cai et al., 2013). In cochlea expressing *Atoh1*-EGFP, the earliest GFP expression is seen as a diffuse, salt-and-pepper patch of cells in the mid-basal

Development (2019) 146, dev177881. doi:10.1242/dev.177881

region at E13.5. In basal cochleae at E16.5, GFP is restricted to cells that express the early HC differentiation marker myosin VI and is localized to one IHC row and three OHC rows (Cai et al., 2013). This suggests that Atoh1 first appears in the prosensory domain as a prosensory factor, and then becomes restricted to developing HCs as a commitment factor responsible for HC fate decision.

Despite these insights into the role of Atoh1 in HC differentiation, several questions remain: within the prosensory domain showing the salt-and-pepper Atoh1 expression pattern, are the prosensory cells with a relatively high level of Atoh1 destined to differentiate into HCs? If so, to what extent do these differentiating HCs migrate to join HC rows; if not, by what means are HCs selected from prosensory cells? To address these questions, it is necessary to trace the fate of the prosensory cells. Lineage tracing using inducible recombinases such as the Cre-LoxP system is not feasible because the region of the prosensory domain expressing diffuse Atoh1 undergoes a dramatic and rapid change into a prototype of the organ of Corti (composed of IHCs, OHCs and the space between) within approximately 2 days, which is too rapid to make use of Cre-LoxP recombination and labeling of fixed samples.

This study was initiated to elucidate how the prototype organ of Corti is formed via differentiation, migration and organization of differentiating cells, and to identify what regulates these processes. To do so, we established a three-dimensional time-lapse imaging system using cochlear explants of transgenic mice carrying fluorescent markers. We used this system to investigate the transition process from prosensory domain to the prototype of the organ of Corti. Two fluorescent markers were employed: green fluorescent protein (GFP) in *Atoh1*-EGFP mice; and three mCherry reporter lines for the visualization of the canonical Notch ligand Delta-like1 (Dll1) as a marker for HC fate decision, Hes5 as a marker for SC fate decision, and histone H2B as a marker of nuclei.

Herein, we provide the first description of the changes in Atoh1 levels using three-dimensional live imaging during the transition of prosensory cells into differentiating HCs; we identified four phases in this transition. In addition, we define the relationship among cells expressing low-level GFP, high-level GFP, Dll1 and Hes5, and confirm that a change in GFP intensity can be interpreted as a cell fate commitment. Our results on cell tracking indicate not only that IHC induction occurs at the medial periphery of the prosensory domain, but also that early OHC induction occurs at the lateral periphery of the prosensory domain, as if to maintain sufficient space between IHCs and OHCs. Our analyses also explain the effects of hedgehog (Hh) and Bmp4 signaling inhibitors on the transition from the prosensory domain to the prototype of the organ of Corti. We propose a model in which multi-directional signals from outside of the prosensory domain regulate the dynamics of OHC induction and organization.

RESULTS

Endogenous Atoh1 expression pattern changes from weak, diffuse, salt-and-pepper expression in prosensory cells to strong expression in developing hair cells

The organ of Corti has epithelial polarities in three orientations: medial-lateral, apical-basal and lumen-basement membrane axes (Fig. 1A). In the following text and figures, the medial-lateral, apical-basal and lumen-basement membrane axes are termed the *x*-axis, *y*-axis and *z*-axis, respectively.

The presence of Atoh1 protein in the developing cochlear epithelium was visualized using a highly sensitive anti-Atoh1 antibody (Yamada et al., 2014) (Fig. 1B-D). Weak Atoh1 expression was first identified at E13.5 and was localized to a patch of cells showing diffuse salt-and-pepper staining in the mid-basal region (Fig. 1B). This observation was consistent with the pattern of GFP expression in *Atoh1*-EGFP mice (Cai et al., 2013). At E14.5, this weak staining pattern extended toward the apical turn (Fig. 1C); in the mid-basal cochlea, intense staining of Atoh1 protein was present at the medial edge of the patch (Fig. 1C,C″). At E16.5 in the apical turn, Atoh1 staining was more intense in a row of cells located at the most medial edge, within a stripe of prosensory cells that showed weak and diffuse Atoh1 staining (Fig. 1D). Cells in the more basal region of the lateral compartment showed stronger Atoh1 staining (compare Fig. 1D′ with Fig. 1D). In the lateral compartment of the middle turn, more cells showed strong Atoh1 staining, but the cells were not organized into clear rows (Fig. 1D″). In the basal cochlea, Atoh1-positive cells in the lateral compartment were organized as three rows of developing OHCs (Fig. 1D‴). The pattern of Atoh1 expression was compatible with the results reported by Chen et al. (2002) and Cai et al. (2013). We also confirmed that GFP intensity in prosensory cells of cochleae of *Atoh1*-EGFP mouse embryos can be interpreted as representative of endogenous Atoh1 levels (Fig. S1).

In order to determine whether weak Atoh1 staining occurred in the prosensory domain, we performed a co-immunolabeling investigation of Atoh1 and the commonly used prosensory markers $p27^{Kip1}$ (also known as Cdkn1b – Mouse Genome Informatics), Sox2 and Hey2. The analysis was carried out using mid-modiolar sections from the basal turn of *Atoh1*-EGFP embryos at E14.5 (Fig. S2A-C). The lateral edge of the weak GFP expression closely corresponded to $p27^{Kip1}$ and Hey2 expression (Fig. S2A-A″,C-C″). $p27^{Kip1}$ and Hey2 were downregulated in cells located at the medial edge of the Atoh1-positive area that expressed stronger GFP. The Sox2-positive area was broader than the GFP-positive area (Fig. S2B-B″). These observations indicate that the initial Atoh1 weakly positive area appears in the $p27^{Kip1}$-positive prosensory domain.

Four phases of Atoh1 expression during the organ of Corti patterning across the radial axis

Endogenous Atoh1 expression changes from a weak, diffuse, salt-and-pepper pattern in prosensory cells to strong expression in developing hair cells (Fig. 1E). This process, which corresponds to the transition from the prosensory domain to the prototype of the organ of Corti (composed of IHCs, OHCs and the space between IHCs and OHCs), can be divided into four phases. In Phase I, Atoh1 expression is weak, diffuse and exhibits a salt-and-pepper pattern. In Phase II, stronger Atoh1 expression appears in cells located at the most medial edge of the Atoh1-positive prosensory area. In Phase III, stronger Atoh1 expression also appears in the lateral compartment of the Atoh1-positive prosensory area. In Phase IV, Atoh1-positive cells are aligned in four rows, indicating IHC and OHC differentiation.

The correlation between Atoh1 expression and prosensory marker Sox2 was analyzed by immunohistochemistry of E14.5 embryos using whole-mounted cochlear samples prepared for a surface view (Fig. S2D-F). The data indicated that weak Atoh1 expression in prosensory cells of Phases I and II was correlated with Sox2 expression (Fig. S2F), whereas strong Atoh1 expression in cells committed to HC fate was not correlated with Sox2 expression (Fig. S2F, circled).

Dynamic changes of Atoh1 expression from Phase I to Phase IV were visualized by two-day three-dimensional real-time imaging of *Atoh1*-EGFP mouse cochlear explants (Fig. 2). A schematic of our three-dimensional time-lapse imaging system is shown in Fig. 2A-D. An example of the results of such an analysis is shown: first, a tile scan of the cochlear epithelium was performed, and an area corresponding to Phase I was chosen for imaging (Fig. 2E, boxed area); next, the gradual transition from Phase I to Phase IV appeared

Development (2019) 146, dev177881. doi:10.1242/dev.177881

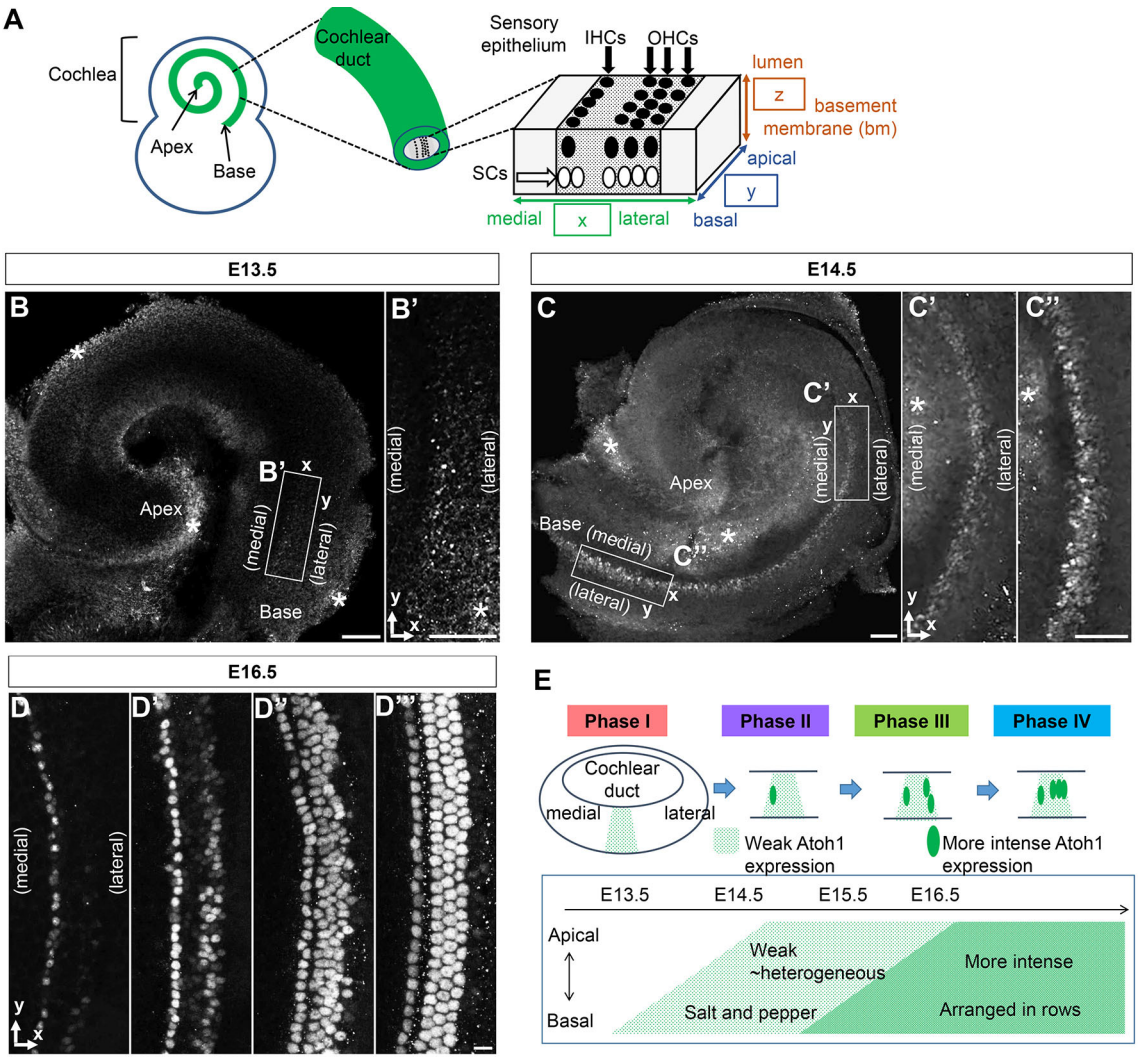

Fig. 1. Atoh1 expression in the developing cochlear epithelium visualized using an anti-Atoh1 antibody and *Atoh1*-EGFP fusion protein. (A) Three-dimensional diagram of cochlear epithelium to indicate the directions of the medial-lateral, apical-basal and lumen-basement membrane axes. IHCs and OHCs are shown by black ovals and indicated by black arrows; SCs are shown by white ovals and indicated by a white arrow. (B-D) Atoh1 expression in the developing cochlear epithelium. (B,B′) E13.5 cochlear epithelium. A magnified view of the boxed region is shown (B′). Asterisks indicate presumed artifacts. (C-C″) E14.5 cochlear epithelium. Magnified views of the boxed regions are shown (C′,C″). Asterisks indicate presumed artifacts. (D-D‴) E16.5 cochlear epithelium, apical turn (D), more basal part of the apical turn (D′), middle turn (D″) and basal turn (D‴). (E) Schematic showing the four phases of Atoh1 expression during patterning of the organ of Corti across the radial axis. Scale bars: 100 µm.

in the image series (Fig. 2F,F′). The GFP intensity of the tracked HCs tended to show a relative increase in GFP expression during Phases I-III, followed by a plateau during Phase IV (Fig. 2G).

Weak Atoh1 expression in prosensory cells during Phase I and the earliest HC selection around the medial edge of the prosensory domain

Time-lapse imaging from Phase I (Fig. 3A) to Phase II (Fig. 3B) was performed using cochlear explants from E13.5 embryos with an *Atoh1*-EGFP; R26-H2B-mCherry genotype. Movie 1 contains *xz* projection images of the time-lapse experiment; Fig. 3B-G shows snapshots of the movie. Spots were detected using Imaris software, based on nuclear mCherry signals in the three-dimensional images (Fig. 3B′-G′). The cells within the Atoh1-positive prosensory domain region gained more GFP intensity than those that were medial or lateral to the prosensory domain (Fig. 3B′-G′). After 11 h, cells with high GFP intensity appeared at the medial periphery of the Atoh1-positive prosensory domain (Fig. 3F,F′,G,G′).

In the time-lapse experiment shown in Fig. 3B-G and Movie 1, cells with high GFP intensity first appeared between 11 h and 15 h, indicating that Phase II began after 11 h. Therefore, cell tracking was performed using images obtained after 11 h in order to determine where these cells originated. Cells with high-GFP intensity were located at 15 h and 19 h adjacent to the medial edge of the Atoh1-positive prosensory domain (Fig. 3H-K). These results indicated that, although Atoh1 expression occurs rather widely at low levels, the cells located at the medial edge are selected to express Atoh1 at high levels to become the earliest HCs, considered to be presumptive IHCs.

Cells tracked for more than 8 h during Phases I and II are shown in Fig. 3L,P and Movies 2 and 3. In order to know whether Atoh1 expression in each prosensory cell steadily increases or fluctuates, the tracks were divided into two groups based on maximum GFP intensity of the cells. GFP intensities in cells 1-3 and 6 increased over 19 h (Fig. 3M,N, Movie 2), suggesting that they are selected as IHCs; the GFP intensities of cells 4, 5, 7 and 8 decreased after an initial

Development (2019) 146, dev177881. doi:10.1242/dev.177881

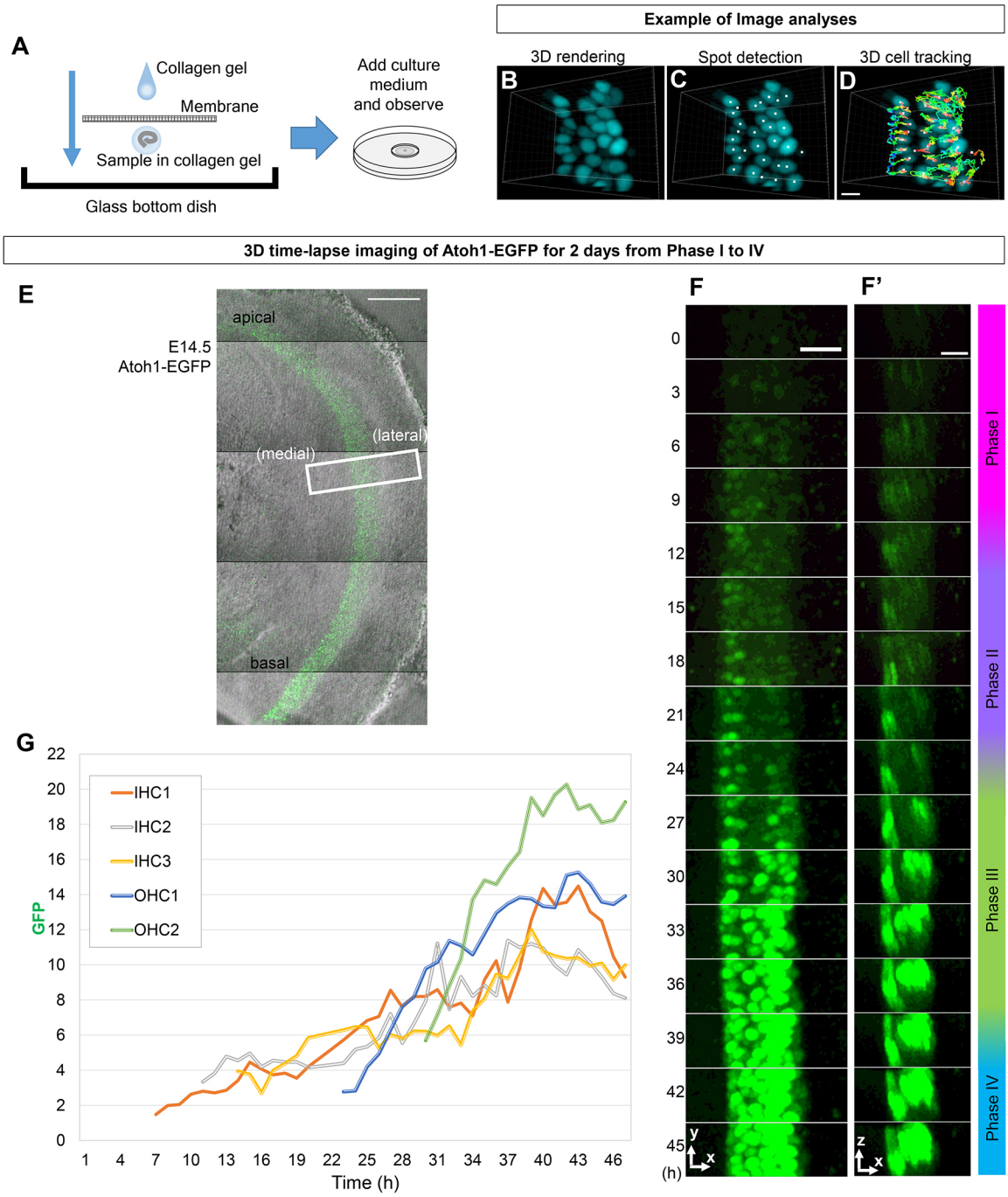

Fig. 2. Time-lapse imaging of *Atoh1*-EGFP expression of the cochlear epithelium. (A-D) Schematic showing the three-dimensional time-lapse imaging system. A shows the setting up of a cochlear culture, and B-D show examples of image analyses by Imaris software: a *z*-stack image series obtained by confocal microscopy was processed using Imaris software to obtain three-dimensional renders (B), spot detection (C) and tracking of individual cells (D). (E-G) A representative three-dimensional time-lapse image. (E) Tile scan of the cochlear epithelium before real-time imaging. The boxed area was chosen for imaging. (F) Three-hourly images of two-dimensional *xy* projections. The depth of the *y* direction is 26.0 µm. (F′) Three-hourly images of two-dimensional *xz* projections. The depth of the *z* direction is 40.1 µm. The color bar indicates the gradual transition from Phase I to Phase IV. (G) The relative GFP intensity of the tracked cells IHC 1, IHC 2, IHC 3, OHC 1 and OHC 2 is plotted per hour. Each line represents the GFP intensity of individual cells. Scale bars: 10 µm in B-D; 100 µm in E; 20 µm in F,F′.

increase (Fig. 3N,O, Movie 3); the GFP intensities of cells 9-12 remained low until the cells were no longer detectable (Fig. 3Q, Movie 3); the GFP intensities of cells 13-16 fluctuated in an asynchronized manner (Fig. 3R). These results suggest that low levels of Atoh1 expression fluctuate randomly in a subset of the Atoh1-positive prosensory cells during Phases I and II, and that the cells that express Atoh1 over a certain threshold are selected to become HCs.

Atoh1 enhancer becomes active in the cells fated to be HCs, not in the prosensory cells before fate determination

Atoh1 positively autoregulates its own expression by binding to an E-box motif in its enhancer complex (Helms et al., 2000). This autoregulation has been shown to be necessary for the continued expression of *Atoh1* in HCs; *Atoh1* mutant mice cannot maintain expression in HCs of a GFP

Development (2019) 146, dev177881. doi:10.1242/dev.177881

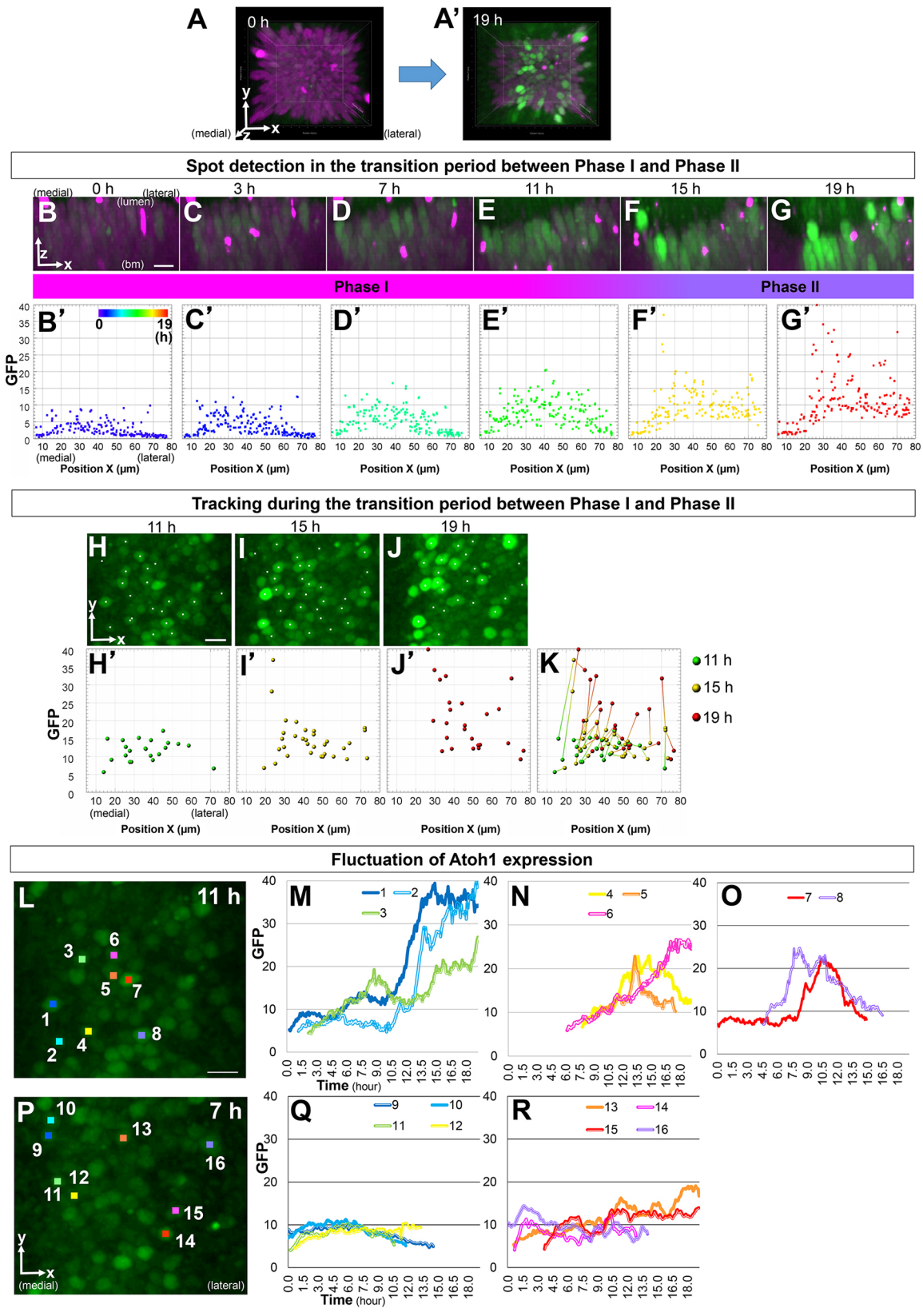

Fig. 3. See next page for legend.

reporter transgene containing the autoregulatory enhancer (Raft et al., 2007).

Transgenic mice carrying EGFP under the control of an enhancer from the *Atoh1* gene (*Atoh1*-nGFP) were previously described (Lumpkin et al., 2003). The transgene contains an ∼1.4 kb sequence from the *Atoh1* enhancer (Helms et al., 2000) and controls the expression of nuclear GFP reporter. In this transgenic mouse, Lumpkin et al. reported that GFP is expressed in Atoh1-positive

Development (2019) 146, dev177881. doi:10.1242/dev.177881

Fig. 3. IHC induction during the transition from Phase I to Phase II. (A,A′) Phase I at the beginning and Phase II at the end of real-time imaging. Three-dimensional rendering of *z*-stack images of E13.5 *Atoh1*-EGFP; R26-H2B-mCherry cochlear explant at the first time frame (0 h) (A) and the time frame at 19 h (A′). View area of *x* direction is 76.1 µm, *y* direction is 64.6 µm and *z* direction is 38.7 µm. (B-G, B′-G′) Spot detection in the transition period between Phase I and Phase II. (B-G) Snapshots of Movie 6, containing *xz* projection images of the time-lapse experiment. (B′-G′) The *x* position and GFP intensity of individual spots detected using Imaris software, based on nuclear mCherry signal in the three-dimensional images, using the same *xz* projection and time points as B-G. The Atoh1-positive prosensory domain was located between 10 and 80 µm of *x* position. Corresponding phases of the Atoh1 expression pattern are shown below panel B-G. The colors of dots stand for the time, and there is a rainbow-color time scale in panel B′. (H-J,H′-J′) Tracking during the transition period between Phase I and Phase II. Cell tracking was performed using images obtained after 11 h in order to identify the origin of cells with high GFP. Cells tracked between 11 h and 15 h and/or 15 h and 19 h are selected among all tracks. The selected tracks in *xy* projection images at 11 h (H), 15 h (I) and 19 h (J). Relative GFP intensity and *x* position of the selected tracks at 11 h (H′), 15 h (I′) and 19 h (J′). (K) The connected plots of individual tracks at 11 h, 15 h and 19 h. (L-R) Fluctuation of Atoh1 expression in individual Atoh1-positive prosensory cells. Sixteen cells were tracked for more than 8 h during Phase I-II. They were divided into two groups, according to maximum GFP intensity of each cell: high maximum GFP and lower maximum GFP. (L) Eight higher maximum GFP cells in the *xy* projection image. Each color of the points is the same as that in Movie 2. (M) The time and GFP intensity of cells 1-3. (N) The time and GFP intensity of cells 4-6. (O) The time and GFP intensity of cells 7-8. (P) Eight lower maximum-GFP cells in the *xy* projection image. Each color of the points is the same as that in Movie 3. (Q) The time and GFP intensity of cells 9-12. (R) The time and GFP intensity of cells 13-16. Scale bars: 10 µm.

domains in HCs in the developing vestibular and auditory systems, and that GFP fluorescence is not detected in the E13.5 cochlea, reflecting the timing of HC differentiation in these tissues (Lumpkin et al., 2003).

Atoh1-nGFP mice can be used for labeling developing HCs in inner ears. Here, we investigated whether the mice could be used to visualize Phase I and II prosensory cells before fate determination (Fig. S2G-I). In the middle turn of E14.5 *Atoh1*-nGFP embryos, little GFP expression was observed in Atoh1-positive prosensory cells and there was no positive linear correlation between Atoh1 and GFP intensity (Fig. S2G,I). We also performed cell lineage tracing using Tg-*Atoh1-Cre* mice (Fujiyama et al., 2009), in which Cre expression is driven by the same Atoh1 enhancer element as *Atoh1*-nGFP mice. In these mice, again only the cells fated to be HCs were labeled (Fig. S2J,K). Thus, marking by the Atoh1 enhancer element only labeled the cells that expressed Atoh1 at high levels and started HC differentiation, suggesting that the *Atoh1* enhancer becomes active in the cells fated to be HCs, not in the prosensory cells before fate determination.

Atoh1-positive cell migration toward lumen precedes HC fate determination

Mice carrying a Dll1-Venus fusion construct and a cleaved mCherry reporter have been generated; in these Dll1-Venus-T2A-mCherry mice, the surface of Dll1-expressing cells is labeled by Venus and the cytoplasm of Dll1-expressing cells is labeled by mCherry (Fig. S3A). We confirmed that visualization of GFP was not affected by Venus fluorescence in double transgenic *Atoh1*-EGFP and Dll1-Venus-2a-mCherry mice (Fig. S3B-E). Time-lapse imaging of cochlear explants from E14.5 *Atoh1*-EGFP; Dll1-mCherry embryos revealed that Dll1 was expressed in cells with high levels of Atoh1 during Phases II and III (Fig. S3F,G), suggesting that high Atoh1 and Dll1 expression is associated with HC fate determination.

Cells in cochlear explants from *Atoh1*-EGFP; Dll1-mCherry mice at Phases II and III were tracked for 19 h. Tracks showing weak to strong GFP expression were selected (Fig. 4A-C and Movies 4 and 5). Representative cells in Fig. 4B,B′,C,C′ and Movies 4 and 5 were relatively close to the basement membrane at the beginning of imaging, and migrated toward the cochlear duct lumen in concert with increased GFP intensity before the increase of mCherry intensity.

Thirteen GFP-positive cells in the lateral compartment were tracked for 19 h until the end of the experiment (Fig. 4D,H). The cells were divided into two groups according to GFP intensity (Fig. 4D-G,H-J). Cells with high GFP increased their intensity earlier than those with low GFP levels (Fig. 4E,F). In cells with high GFP levels, *z* position displacement toward the luminal side tended to occur earlier than the increase in mCherry intensity (Fig. 4F,G). Some cells, which had low GFP levels, initially moved toward the lumen and then returned to the side of the basement membrane. GFP intensities in these cells increased initially and then plateaued (Fig. 4I,K: Cells 8 and 9). These results suggest that high *Atoh1*-EGFP and Dll1-Venus-T2A-mCherry levels correspond to Dll1 upregulation and HC fate determination, and that migration of cell nuclei toward the luminal surface precedes Dll1 upregulation and HC fate determination.

Cell fate determination correlated with GFP intensity

Next, we generated pHes5-NLS3-mCherry mice to visualize Hes5 promoter activity and to label the cells fated to differentiate into SCs (Fig. S4, Movie 6). Time-lapse imaging of cochlear explants of *Atoh1*-EGFP; pHes5-mCherry embryos revealed that cells with high GFP were committed to an HC fate, whereas those with either no or low GFP were committed to an SC fate (Fig. S4E-N). There were also some cells with an intermediate GFP level, the fate commitment of which remains undetermined (Fig. S4J,N,O and Movies 7 and 8).

Here, we summarized the results described above (Fig. 5A). The Atoh1-positive prosensory domain is formed within the Sox2-positive prosensory domain. Atoh1 expression in prosensory cells is initially weak and gradually increases over time. Once prosensory cells gain strong Atoh1 expression, they migrate toward the luminal side of the epithelium and begin to express Dll1. On the other side, the prosensory cells that maintain weak Atoh1 expression start to express Hes5, presumably because of Notch lateral inhibition. The timing of fate determination varies; during Phase III, neutral cells that express intermediate levels of Atoh1 and Hes5 remain in the Atoh1-positive prosensory domain. These cells might be used for fine adjustment to form rows of HCs or SCs during later development. Thus, cell fate determination is controlled over time depending on Atoh1 expression levels.

Potential OHC induction models: unidirectional or multi-directional signal models

It is generally accepted that there is a gradient of differentiation along the medial-lateral axis of the cochlea from IHCs to OHCs, resulting in IHCs differentiating earlier than OHCs (Fujiyama et al., 2009; Jones and Jones, 2011). There are two potential models that can account for OHC induction (Fig. 5B,C). First, the unidirectional signal model suggests that a signal from the medial side causes OHCs to differentiate from the medial to lateral side (Fig. 5B). This model is easy to conceptualize, but does not explain the space observed between IHCs and OHCs. Second, the multi-directional signal model suggests that OHCs differentiate from the lateral side and that signals are potentiated from both the medial and lateral

Development (2019) 146, dev177881. doi:10.1242/dev.177881

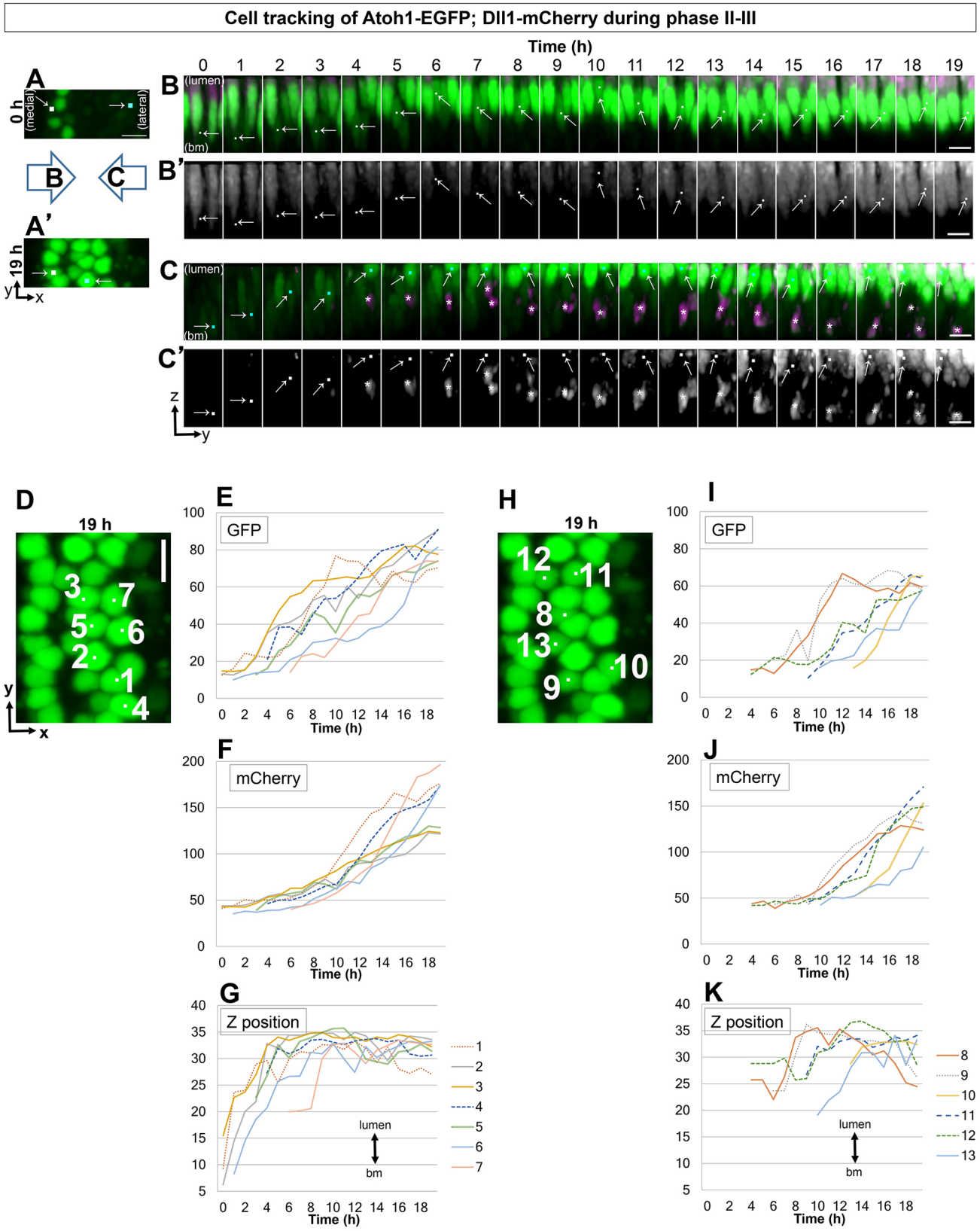

Fig. 4. See next page for legend.

sides (Fig. 5C). This model can explain the space between IHCs and OHCs. The first OHC appearance occurs between E14.5 and E15.5, before pillar cell development mediated by Fgf8-Fgfr3 signaling. Tracking cells that differentiate to an OHC fate during this period might help to resolve how these cells differentiate and to evaluate these opposing models.

Development (2019) 146, dev177881. doi:10.1242/dev.177881

Fig. 4. Cell tracking of *Atoh1*-EGFP; Dll1-mCherry during Phase II-III. (A-C) Representative tracks showing weak to strong GFP expression. (A,A′) *xy* projection images at 0 h (A) and 19 h (A′), respectively, of two representative cells: a presumptive IHC indicated by white dots accompanied by arrows; and a presumptive OHC indicated by cyan dots accompanied by arrows. The cochlear explant was established at E14.5. (B,B′) *yz* projection images viewed from the medial side (the orientations are denoted by the arrows between panels A and A′), and a sequence of frames (one per hour) from Movie 4, focusing on the presumptive IHC indicated by white dots. The depth of the *x* direction is 18.8 µm. (C,C′) *yz* projection images viewed from the lateral side (the orientations are denoted by the arrows between panels A and A′), and a sequence of frames (one per hour) from Movie 5, focusing on the presumptive OHC indicated by cyan dots. The depth of the *x* direction is 26.3 µm. Asterisks indicate presumed artifacts because their shapes do not resemble those of nuclei. B and C show GFP (green) and mCherry (magenta); B′ and C′ show mCherry (white). (D-K) Tracking of GFP-positive cells in the lateral compartment. Tracked cells were divided into two groups according to GFP intensity at 19 h. (D) High GFP cells numbered 1-7. GFP intensity (E), mCherry intensity (F) and *z* position (G) of high GFP cells. Each cell number indicated in G is the cell shown in D, and every color of the lines in E-G corresponds to one cell shown in D. (H) Low GFP cells, numbered 9-13. GFP intensity (I), mCherry intensity (J) and *z* position (K) of low GFP cells. Each cell number indicated in K is the cell shown in H, and every color of the lines in I-K corresponds to one cell shown in H. Scale bars: 10 µm.

OHC production begins near the lateral border of Atoh1-positive prosensory domain

To investigate the order of OHC differentiation, GFP-positive cells in cochlear explants from *Atoh1*-EGFP embryos were tracked from Phase II. A representative experiment is shown in Fig. 5D-N and D′-N′. The tracks of Atoh1-positive cells were divided into six evenly sized groups based on time of first emergence and are distinguished using different colors (Fig. 5D-N and D′-N′, Movies 9-12). OHCs first appeared between 2 h and 4 h and were restricted to the location adjacent to the lateral border of the Atoh1-positive prosensory domain (cyan dots in Fig. 5F,F′). In the subsequent 2 h, OHCs with white dots similarly appeared near the lateral border (Fig. 5G,G′). OHCs shown as yellow, magenta and red dots were induced to more medial and lateral positions, relative to the earlier-appearing spots (Fig. 5H-N,H′-N′). The early OHCs that emerged from the lateral edge of the Atoh1-positive prosensory domain migrated toward medial position (cyan and white dots in Fig. 5H-N,H′-N′), whereas later OHCs first emerged at more medial and lateral positions. Taken together, OHC production begins near the lateral border of Atoh1-positive prosensory domain, and thereafter, OHCs are derived from multiple positions in the lateral region of the prosensory domain. Thus, in addition to the IHC-producing Atoh1-high medial region, there appeared to be a lateral-high and medial-low gradient of Atoh1 expression in the OHC-producing region, supporting the multi-directional signal model.

Bmp4 inhibitors disrupt Atoh1 expression pattern in the developing sensory epithelium

In the multi-directional signal model, it is implied that there are signals to downregulate Atoh1 between the prospective IHC and OHC areas and upregulate Atoh1 in the prospective OHC area. We presumed that the transient inhibitory signal is Shh, a negative regulator for HC differentiation (Bok et al., 2013; Tateya et al., 2013), which comes from the spiral ganglion. We also hypothesized that Bmp4 is involved in the lateral signal to upregulate Atoh1 because Bmp4 is expressed in the cochlear epithelium lateral to the prosensory domain (Fig. S5A) (Ohyama et al., 2010). The Bmp4 inhibitor LDN193189 was used to elucidate the Bmp4 signaling pathway in prosensory cells. E13.5 *Atoh1*-EGFP cochleae were cultured for 2 days with or without LDN193189 (Fig. S5B-H). In negative control cochlea, the apical turn was Phase II (Fig. S5C) and the middle and basal turns were Phase III (Fig. S5D,E). In contrast, in the middle and basal turns of the cochlea cultured with LDN193189, Atoh1 expression within the lateral prosensory domain remained weak and OHC differentiation was suppressed (Fig. S5G,H). This result suggested that Bmp4 is necessary for Atoh1 upregulation in the lateral prosensory domain.

Initial Atoh1 expression in the prosensory domain to induce early OHCs was disrupted by Hh or Bmp4 inhibition

Next, to evaluate the roles of Shh signaling and Bmp4 signaling in Atoh1 expression and patterning of the prototypic organ of Corti, live imaging was performed with cyclopamine, an Shh inhibitor, or LDN193189. The standardization of time and fluorescent signal was performed by an algorithm to detect ‘first emerging position’ (FEP), that is, the first appearance of developing OHCs, in order to make the comparison and the statistical analyses among time-lapse imaging experiments.

We first generated X-t kymographs of *Atoh1*-EGFP signals and defined FEP of Atoh1-positive signals in the *x*-axis. Fig. 6A-C shows the representative X-t kymographs of the control experiment and the experiments with cyclopamine or LDN193189, respectively. In the control shown in Fig. 6A, GFP intensity was raised initially at the medial periphery of Atoh1-positive prosensory domain, and then GFP intensity became more intense at the opposite periphery of the prosensory domain. Administration of both cyclopamine and LDN193189 significantly medialized FEP, though the standard variation of FEP became larger than the control following treatment with cyclopamine or LDN192189 (Fig. 6B-D).

Next, we defined the ‘medial area’ and ‘lateral area’ to quantify the medial-lateral gradient of initial Atoh1 expression in the prospective OHC area, and calculated mean GFP intensity for 1 h after the time of FEP. In the control experiments, GFP intensity in the lateral area was significantly higher than that in the medial area. It means that there is a lateral-high and medial-low gradient of Atoh1 expression in the prospective OHC area (Fig. 6E,F). Contrary to the control, GFP intensity in the lateral area became significantly lower than that in the medial area following treatment with cyclopamine, and was not significantly different from that in the medial area following treatment with LDN191893 (Fig. 6F). It means that the initial lateral-high and medial-low gradient of Atoh1 expression in the prospective OHC area was disturbed by Shh inhibition or Bmp4 inhibition (Fig. 6F).

Finally, we performed three-dimensional cell tracking in E14.5 *Atoh1*-EGFP cochlear explants based on the time standardization using FEP (FEP=0). A representative experiment is shown in Fig. S6A-I and Movies 13-15. When cyclopamine or LDN193189 was administered to the cochlear explant, the initial spots that appeared were not restricted to the position near the lateral edge of Atoh1-positive prosensory domain as the case in control (Fig. S6D-F and Movies 13-15).

This tendency of the first OHC spots was also confirmed by the correlation between time and distance from the average IHC position (Fig. S6J-L). There was a negative correlation between time and distance from IHCs in control experiments ($r=-0.25$, $P<0.05$) (Fig. S6J). This result indicates that OHCs are initially induced in the lateral part of the prosensory domain and thereafter induced in the more medial part as well as the lateral part of the prosensory domain. On the other hand, there was no significant correlation between time and distance of initial OHC spots in the samples treated with cyclopamine ($r=0.11$) (Fig. S6K), and there was a positive correlation in the samples treated with LDN193189

Development (2019) 146, dev177881. doi:10.1242/dev.177881

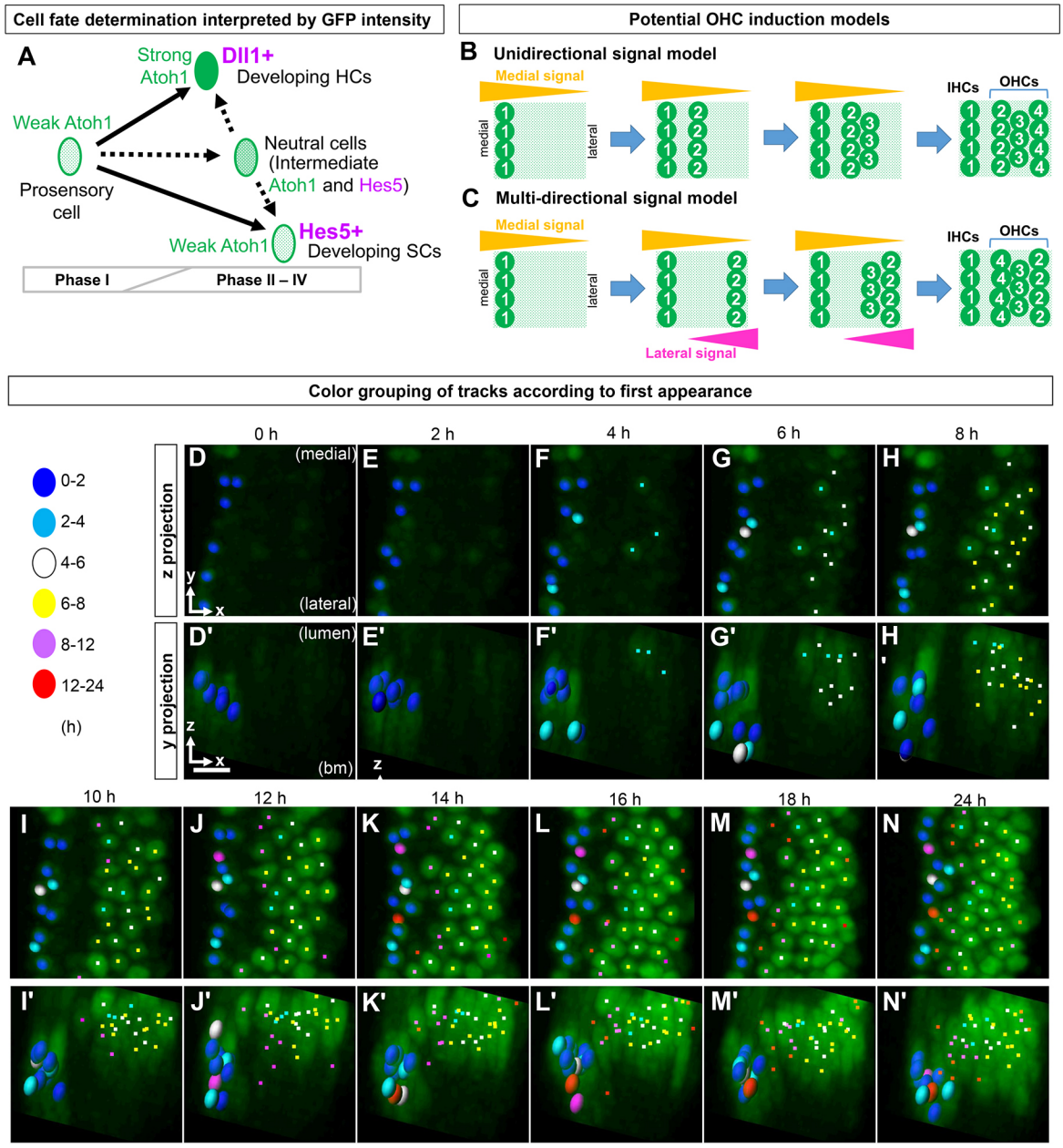

Fig. 5. OHC induction during the transition from Phase II to Phase III. (A) Cell fate determination as interpreted by GFP intensity. Summary of the results previously described. (B,C) Potential OHC induction models: widely accepted unidirectional model (B) or multi-directional signal model (C). (D-N,D′-N′) Color grouping of tracks according to first emergence. Forty-eight tracks of Atoh1-positive cells were divided into six evenly sized groups based on time of first emergence and are shown using different colors. The cochlear explant was established at E14.5. The tracks that appeared between 0-2 h, 2-4 h, 4-6 h, 6-8 h, 8-12 h and 12-24 h are marked by blue, cyan, white, yellow, magenta and red, respectively; spheres indicate IHCs and dots indicate OHCs. Because the epithelium was oblique, the images are rotated 10° on the *y*-axis. (D-N) Snapshots of Movie 10, containing *xy* projection images of the time-lapse experiment. (D′-N′) Snapshots of Movie 12, containing *xz* projection images of the time-lapse experiment. Scale bar: 10 µm.

(r=0.24, P<0.05) (Fig. S6L). These results indicate that the pattern of initial OHC appearance was disturbed by Shh inhibition or Bmp4 inhibition. These results are summarized in Fig. 7A,B.

DISCUSSION

Model for initial OHC patterning across the medial-lateral axis

The proposed model in this study is shown in Fig. 7C. Our data support the multi-directional model shown in Fig. 5C, with some modifications. First, IHCs begin to differentiate as a result of a medial signal (Fig. 7C). Shh signaling from the spiral ganglion inhibits Atoh1 elevation, which makes the space between the IHC and OHC areas. Shh from the spiral ganglion is known to suppress HC differentiation; in addition, Shh disappears from the basal turn to the apical turn, as HC differentiation proceeds (Bok et al., 2013), indicating that Shh inhibits HC differentiation in the lateral compartment. As Shh expression decreases, OHC differentiation begins at the lateral periphery. The area in which OHCs are induced then expands toward the medial side. When Shh signaling is inhibited, or after Bmp4 signaling is inhibited, OHCs appear across the whole prosensory domain and Atoh1 is upregulated initially in medial prosensory cells (Fig. 7B).

Development (2019) 146, dev177881. doi:10.1242/dev.177881

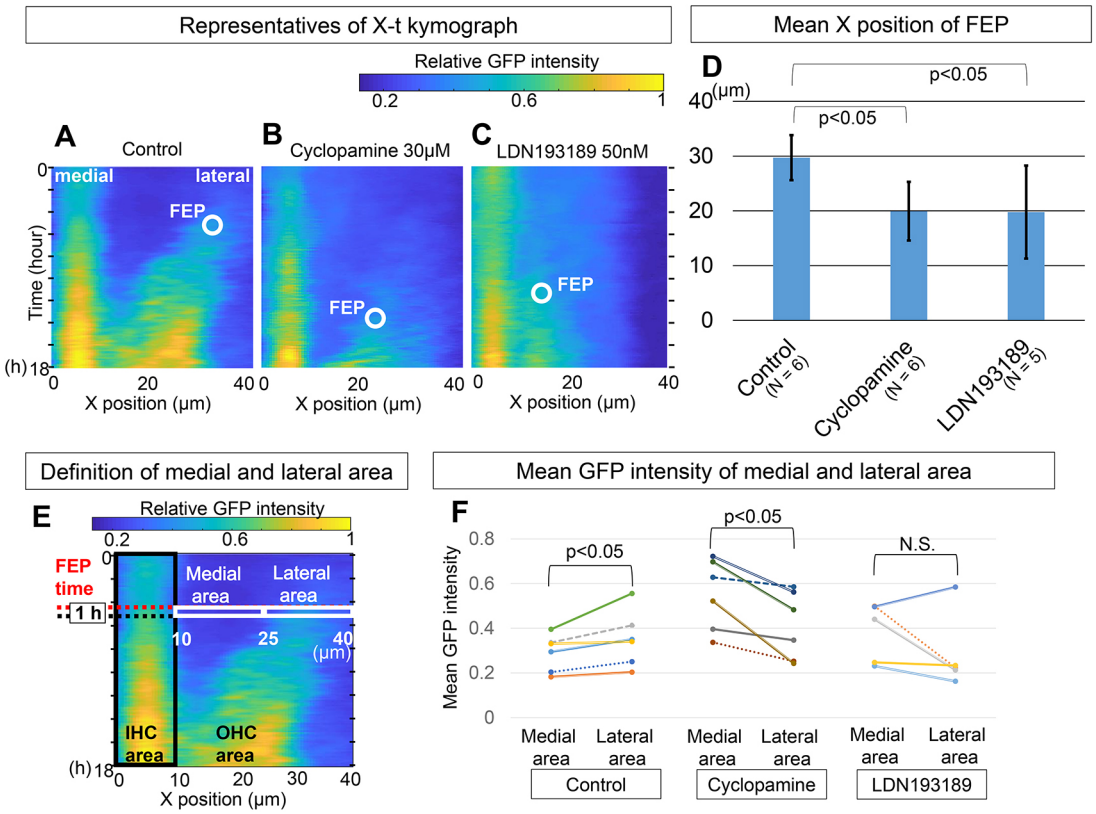

Fig. 6. The FEP of Atoh1-positive signals in the *x*-axis defined for the quantitative analysis of 3D live imaging data. (A-C) A representative X-t kymograph of *Atoh1*-EGFP signals and FEP of Atoh1-positive signals in the *x*-axis in control (A), and following treatment with cyclopamine (B) or LDN193189 (C). FEP is indicated as circles. The cochlear explants used for the analysis of FEP were established at E14.5. (D) Mean *x* position of FEP. *x* position of control experiments is significantly more lateral than those of the cyclopamine experiments and the LDN103189 experiments (P<0.05). (E) Definition of the 'medial area' and 'lateral area'. (F) Mean GFP intensity of the medial and lateral area, 1 h after the time of FEP. In the control experiments, GFP intensity in the lateral area was significantly higher than that in the medial area (P<0.05). Contrary to the control, GFP intensity in the lateral area became significantly lower than that in the medial area in the experiments with cyclopamine (P<0.05), and there was no significant difference (N.S.) between the medial and lateral area in the experiments with LDN193189.

Multi-directional signals in prosensory domain temporally keep a space for pillar cells and the tunnel of Corti

GFP-positive cell tracking revealed that HC induction initially occurs at the medial and lateral periphery of the prosensory domain, as if to maintain sufficient space to form pillar cells and the tunnel of Corti between the IHCs and OHCs. At least three signals from outside of the prosensory domain affect HC differentiation to form the prototype organ of Corti. The signal from the medial side has been suggested to involve the Wnt pathway (Munnamalai and Fakete, 2016). Wnt activation can promote IHC fate determination and, in addition, Wnts can suppress OHC fate determination by antagonizing Bmp4 (Munnamalai and Fakete, 2016). In the present study, we show that Bmp4 expression at the lateral periphery of the prosensory domain promotes OHC fate. In addition to medial Wnt and lateral Bmp4, Shh signaling from the spiral ganglion negatively regulates HC differentiation (Bok et al., 2013; Tateya et al., 2013). Shh signaling has a greater influence on the OHC fate than on the IHC fate (Tateya et al., 2013) and may segregate IHCs and OHCs by inhibiting OHC differentiation.

We found that inactivation of Shh signaling caused deformity within the HC rows as well as a reduction in the number of OHC rows; cells with U-shaped stereocilia, which resembled IHCs, were present within the rows of OHCs that have V-shaped stereocilia (Tateya et al., 2013). Weak expression of the pillar cell marker $p75^{NTR}$ (Ngfr – Mouse Genome Informatics) was observed in SCs, between ectopic IHCs with U-shaped stereocilia and OHCs (Tateya et al., 2013). This finding suggests that ectopic IHCs with U-shaped stereocilia were accompanied by ectopic pillar cells, causing the above-mentioned deformity of the tunnel of Corti. Further, the abnormal mixture of IHCs and OHCs and disruption of the tunnel of Corti formation observed following Shh inactivation resulted from incomplete segregation of IHCs and OHCs; HC induction began across the whole prosensory domain, not at its medial and lateral edges, resulting in an insufficient space for formation of pillar cells and the tunnel of Corti.

Atoh1 regulation by Hh and Bmp signaling is involved in HC induction before Notch-mediated lateral inhibition and Fgf8-Fgfr3 activation

Notch-mediated lateral inhibition and Fgf8-Fgfr3 signaling are well-known pathways to regulate HC and SC differentiation (Kelly and Chen, 2009; Wan et al., 2013). Notch ligands activate Notch signaling in neighboring cells, and activation of Notch signaling leads to expression of repressor genes such as Hes1 and Hes5, thereby inducing adoption of a fate different from Notch ligand-expressing cells (Kageyama et al., 2007). In embryonic mouse cochleae, the initial expression of the Notch ligands such as Dll1 and Jagged2 (Jag2) is observed between E14.5 and E15.5 and is restricted to a single row of cells located in the region of the epithelium that will develop as IHCs. The expression of Dll1 and

Development (2019) 146, dev177881. doi:10.1242/dev.177881

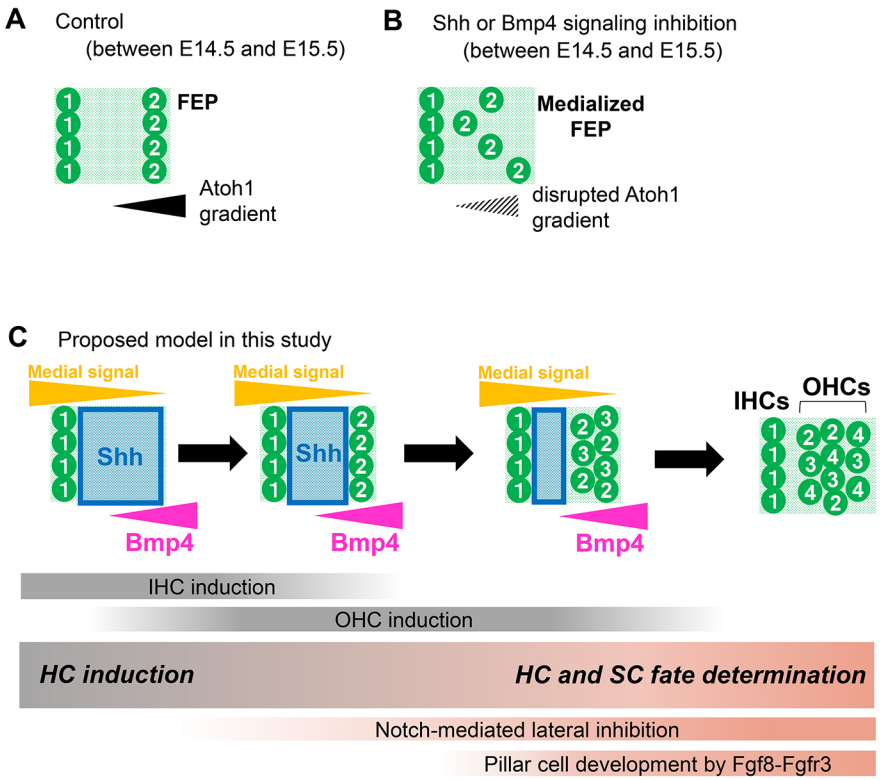

Fig. 7. Summary and proposed model.
(A,B) Summary of quantitative analyses using X-t kymograph showing control experiments (A), and Shh and Bmp4 signaling inhibition (B). (C) Proposed model in this study.

Jag2 is belatedly visible in an additional three parallel rows of cells corresponding to the future OHCs (Lanford et al., 1999; Morrison et al., 1999). On the other hand, SCs express the Notch effector genes such as *Hes1*, *Hes5* and *Hey1* (Zheng and Gao, 2000; Zine et al., 2001; Hayashi et al., 2008; Li et al., 2008). Genetic ablation of Notch ligand or effector genes leads to overproduction of HCs (Kiernan et al., 2005; Tateya et al., 2011). These results suggest that Notch-mediated lateral inhibition regulates HC versus SC specification. However, lateral inhibition stabilizes HC selection but does not initiate HC differentiation. What induces the expression of Notch ligands in the cells that will differentiate into HCs is still unknown. It is believed that the cells selected to differentiate into HCs express the factors involved in HC induction before Notch ligands.

Fgf8-Fgfr3 signaling is reported to regulate pillar cell development. Fgf8 from developing IHCs induces the neighboring Fgfr3-positive cells to differentiate into pillar cells (Shim et al., 2005; Hayashi et al., 2007; Jacques et al., 2007; Puligilla et al., 2007). Fgf8 expression is first observed in developing IHCs of the basal turn at E15.5 and sweeps from base to apex over the next three days (Hayashi et al., 2007). It indicates that pillar cells are induced after OHC induction. Our results also suggest that, at the first appearance of OHCs, there is already a space between IHCs and OHCs in which pillar cells will arise and then the tunnel of Corti will be formed, and conversely, at this time point it is difficult to distinguish OHCs from IHCs without the space.

Thus, we believe that both Notch-mediated lateral inhibition and Fgf8-Fgfr3 signaling are not sufficient to explain what induces HC differentiation and what separates OHCs from IHCs. Our results suggest that dynamic Atoh1 expression regulated by Hh signaling and Bmp signaling is involved in OHC induction and initiation of prototype formation of the organ of Corti, and Notch-mediated lateral inhibition and Fgf8-Fgfr3 signaling take over HC and SC fate determination so as to confirm the prototype of the organ of Corti. The periods when these signaling pathways act are schematically shown in Fig. 7C and may partially overlap one another.

Atoh1 fluctuation in prosensory cells and positive feedback via the Atoh1 enhancer to initiate HC differentiation

Our study suggests that a salt-and-pepper pattern of Atoh1 in the prosensory domain is caused by Atoh1 fluctuation within each prosensory cell; further, the *x* position appears to be more important for HC induction than relative Atoh1 expression levels. For example, cell 7 in Fig. 3L,O expressed a relatively higher level of Atoh1 than other cells at 11 h, but was located at the center of the prosensory domain. HC induction occurred in more medial cells, such as cells 1 and 2, and Atoh1 in cell 7 was then downregulated. Nevertheless, the cells that express relatively high Atoh1 may be chosen as presumptive HCs among the cells at the same *x* position in response to an HC differentiation signal. Our data suggest that activity of the Atoh1 enhancer is a cue to initiate HC differentiation, and that the cells that express Atoh1 over a certain threshold, depending on the Atoh1 enhancer, differentiate into HCs. A steep increase in Atoh1 expression was observed in presumptive HCs and it is likely that there was positive feedback via an Atoh1 enhancer. Abdolazimi et al. (2016) presented the model of Atoh1 regulation during organ of Corti development; once the Atoh1 autoregulatory threshold is achieved in selected nascent hair cells, Notch-mediated active repression is triggered in the surrounding prosensory cells to stimulate the silencing of Atoh1 through Hes/Hey binding to the repressive Atoh1 promotor region, leading to the onset of supporting cell differentiation and the patterning of the cellular mosaic of the organ of Corti. This model is compatible with our findings.

Ahmed et al. reported that Sox2 is required for directly activating Atoh1 transcription in prosensory cells, but once Atoh1 is highly expressed and prosensory cells begin to differentiate into hair cells, Sox2 expression is downregulated in nascent hair cells from E15.5

Development (2019) 146, dev177881. doi:10.1242/dev.177881

and disappears in more mature hair cells (Ahmed et al., 2012). Our results also support this; Sox2 and Atoh1 expression was positively correlated in prosensory cells, but once Atoh1 expression exceeded a certain level, Sox2 did not keep up with Atoh1 increase (Fig. S2D-F). This implies that Sox2 downregulation in developing hair cells occurs after the onset of Atoh1 positive feedback.

Three-dimensional time-lapse imaging complements the existing literature about HC differentiation in the developing cochleae

Time-lapse imaging is a powerful method for analysis of temporal changes in gene expression and positions of individual cells. In the present study, we established the first protocol for three-dimensional time-lapse imaging of cochlear explants. The imaging conditions and time lengths were sufficient to track cells beginning with a prosensory phenotype to their eventual fate as HCs or SCs. We elucidated the dynamics of IHC and OHC induction and organization in the developing cochlea. Such data are extremely difficult to obtain with traditional methods using conventionally fixed and stained specimens.

MATERIALS AND METHODS

Mouse breeding

Atoh1-EGFP fusion (Rose et al., 2009), Tg-*Atoh1-Cre* (Fujiyama et al., 2009), R26-CAG-LoxP-mTFP1 (Imayoshi et al., 2012), *Venus-Hes5* fusion (Imayoshi et al., 2013) and R26-H2B-mCherry (Abe et al., 2011) (CDB0239K) mice were generated as previously described. Generation of the Dll1 C-terminal Venus-T2A-mCherry fusion reporter knock-in constructs (Fig. S3A) was conducted using BAC recombination (Lee et al., 2001; Warming et al., 2005). The BAC clone RP23-306J23 was selected from the Ensembl database (http://www.ensembl.org), and obtained from the BACPAC Resources Center at the Children's Hospital Oakland Research Institute (CHORI). BAC DNA was transferred from the DH10B strain to the SW105 strain by electroporation. The identity and integrity of these BAC clones were verified by a panel of PCR primers and restriction digestions. The Venus-T2A-mCherry reporter coding sequence was amplified using PCR, and cloned into the pBluescript II SK+ plasmid. An frt-PGK-EM7-Neo-frt cassette was inserted behind the reporter coding sequence. The *Neo* gene is driven by both the PGK promoter for G418 selection in ES cells and the EM7 promoter for Kan selection in *Escherichia coli*. A BAC-targeting vector was generated by cloning 300-500 bp homology arms from the *Dll1* gene into a reporter plasmid, flanking the frt-Neo-frt-reporter cassette. The stop codon sequence of *Dll1* was removed. The BAC targeting cassettes were excised by restriction digestion, and electroporated into competent SW105 cells containing the BAC clone of interest. The targeted BAC clone was selected for KanR, and correctly targeted BAC clones were identified using a panel of PCR primers and restriction digestions. We used the pMCS-DTA retrieval vector (a gift from Dr Kosuke Yusa, Osaka University, Japan) as the backbone of our knock-in vectors. pMCS-*DTA* contains the diphtheria toxin fragment-A (*DTA*) gene driven by the MC1 promoter for negative selection in embryonic stem (ES) cells. The knock-in cassette fragment was retrieved from the modified BAC clone into pMCS-*DTA*. The 5′- and 3′-homology arms in the retrieval vector were designed in order that 2.5- or 7.6-kb DNA segments flanking the Venus-T2A-mCherry reporter-frt-PGK-EM7-Neo-frt cassette in the BAC clone could be subcloned into pMCS-*DTA*. The shorter homology arm was used to design PCR-based screening for targeted ES cells (TT2). Chimeric mice were produced from successfully targeted ES cell clones by aggregation with ICR embryos. Germ line transmission of the targeted allele was assessed by PCR of tail DNA. The chimeric mice were crossed with pCAG-FLPe mice (Kanki et al., 2006) to remove the frt-PGK-EM7-Neo-frt cassette.

The pHes5-NLS3-mCherry reporter construct (Fig. S4A) was generated using a 3 kb region of the 5′-flanking sequence, 2 kb of downstream sequence and the SV40 late poly-A adenylation sequence. Three copies of the nuclear localization signal (NLS) of the SV40 large T-antigen were attached to mCherry. To prepare the DNA fragments for pronuclear injection, the vector backbone sequences were removed. The constructs were isolated using agarose gel electrophoresis, purified with QIAEX II (Qiagen) and injected into the pronuclei of fertilized one-cell eggs from ICR mice. Typically 200-300 fertilized eggs were injected. Genotypes were determined by PCR of tail DNA.

These mice were maintained on a C57BL/6;ICR mixed background. The date of vaginal plug identification was defined as E0.5. All mice used in this study were handled in accordance with the Kyoto University Guide for the Care and Use of Laboratory Animals.

Histochemistry and *in situ* hybridization

Whole heads (E13.5-E15.5) or inner ears (E16.5 and older) were fixed in 4% paraformaldehyde in 0.1 M phosphate-buffered saline (PBS) (pH 7.4), cryoprotected in 30% sucrose in PBS and embedded in optimal cutting temperature compound for cryostat sectioning. Immunostaining of cochlear sections was performed as previously described (Imayoshi et al., 2008). The primary antibodies used in this study were rabbit anti-Atoh1 (1:200; a kind gift of Prof. Hoshino, National Center of Neurology and Psychiatry, Japan), rabbit anti-myosin VIIA (1:200; 25-6790, Proteus Bio-Sciences), rabbit anti-Sox2 (1:200; AB5603, Millipore), rabbit anti-Hey2 (1:100; 10597-1-AP, Proteintech), rabbit anti-p75^{NTR} (1:200; 839701, BioLegend), mouse anti-p27^{Kip1} (1:200; 610241, BD Transduction Laboratories), rat anti-GFP (1:200; GF090R, Nacalai Tesque), chicken anti-GFP (1:200; ab13970, Abcam), rabbit anti-DsRed (1:400; 632496, Clontech), rat anti-mCherry (1:200; M11217, Invitrogen), and rat anti-HA (1:200; 11867423001, Roche). Goat anti-species IgG conjugated with Alexa 488 or Alexa 594 were used as secondary antibodies (ab150077, ab150080, ab150116, ab150160, ab150169, Abcam). Nuclei were stained with 4,6'-diamidino-2-phenylindole (DAPI). For p27^{Kip1} and Hey2 staining, samples were heated in 10 mM sodium citrate at 90°C for 10 min before the staining procedure (Tateya et al., 2011). For staining of whole-mounted cochlear preparations, cochlear ducts were opened to expose the developing sensory epithelia prior to the staining procedure (Yamamoto et al., 2009). Actin filaments were visualized with Alexa488 conjugated phalloidin (1:200; A12375, Invitrogen). Stained tissues were photographed using LSM510/780/880 confocal microscopes (Zeiss). *In situ* hybridization was carried out using mouse *Bmp4* probes, as has been previously described (Imayoshi et al., 2008).

Cochlear explant cultures

Cochleae were dissected from mouse embryos and the cochlear epithelium with attached spiral ganglion, and mesenchyme was removed mechanically from the cochlear bone. The cochlear duct was opened, and the surface of the epithelium was exposed. The cochleae were placed onto culture inserts (Millipore) and cultured in DMEM/F-12 supplemented with 3 mg/ml glucose and 0.1 mg/ml ampicillin; 50 nM LDN193189 (Stemgent) was used for Bmp4 signaling inhibition.

Time-lapse imaging

Cochleae were dissected in the same way as for cochlear explant cultures, but the apical turn was resected to flatten the specimen. Cochleae were immersed in type I-A collagen gel (Cellmatrix, Nitta Gelatin; diluted to 2.5 mg/ml collagen, 135 mM NaCl, 5 mM KCl, 1 mM $CaCl_2$, 1 mM $MgCl_2$ and 30 mM HEPES, modified according to the manufacturer's instructions and kept on ice until use) on a glass-bottom dish. Fig. 2A showed the setting up of the cochlear culture; the cochlear epithelium was embedded in a small amount of collagen gel upside-down on the bottom of a glass-bottom dish to bring the luminal surface of the epithelium into contact with the glass surface of the culture dish. A membrane cut out from a culture insert (Millipore) and one more droplet of collagen gel was mounted over the cochlea on the dish to press down the cochlear epithelium.

After 10 min incubation at 37°C, culture medium (the same as that for cochlear explant cultures) was added to the glass-bottom dish, which was then placed on the stage of an inverted confocal microscope and maintained at 37°C in 5% CO_2. Three-dimensional time-lapse images were collected using an inverted confocal laser scanning microscope, LSM 710, 780 or 880 (Carl Zeiss), with a 40× Plan-Apochromat objective (1.4 NA) oil-immersion lens. *Z*-stack images were collected with a 1.1-2.0 µm (mean 1.4 µm) step, at

Development (2019) 146, dev177881. doi:10.1242/dev.177881

3-13 min (mean 5.8 min) intervals for up to 48 h (Table S1). GFP and mCherry fluorescent protein signals were activated by a 488-nm Argon laser and 561-nm Diode Pumped Solid State laser, respectively. GFP images were acquired with the photon-counting mode to reduce laser toxicity. Laser output in a confocal microscope varies between time-lapse imaging sessions; in general, it is highest just after exchange of the laser. Therefore, imaging conditions were modified for each imaging session (Table S1). Experiments were repeated at least four times per genotype of transgenic mice to confirm that comparable results could be obtained. Nevertheless, statistical analysis was difficult.

Shh inhibitor cyclopamine (Enzo Life Sciences) was added to the culture medium at a final concentration of 30 µM, and Bmp4 inhibitor LDN193189 (Stemgent) was added at a final concentration of 50 nM.

Spot detection and tracking using Imaris software

Imaris software (Bitplane) was used for image analyses. To process image sequence files obtained by three-dimensional time-lapse imaging, median filtering and Gaussian filtering were applied to reduce noise. GFP of *Atoh1*-EGFP, mCherry of R26-H2B-mCherry and mCherry of pHes5-NLS3-mCherry are localized to the nuclei, and Imaris recognizes the nuclei labeled by fluorescent proteins as 'spots'. For fluorescent intensity measurement of individual cells, the average intensity inside each spot was calculated. Correlation between two fluorescent proteins was calculated using the relative fluorescent intensity obtained by spot analysis.

Imaris automatically tracks cells by connecting spots in a time series of three-dimensional images. The accuracy of the automated tracking was manually verified and modified when the connection between spots was incorrect.

Quantitative analyses of the data obtained by live imaging

Next, to evaluate the roles of Shh signaling and Bmp4 signaling in Atoh1 expression and patterning of the prototypic organ of Corti, live imaging was performed with cyclopamine or LDN193189. There is a problem to be solved to evaluate the effects of these inhibitors on Atoh1 expression and patterning; every time-lapse imaging is different in the experimental condition (Table S1). Hair cell differentiation starts in the mid-basal region of the cochlea and then proceeds toward the apex until it covers the entire length of the sensory epithelium, like a basal-to-apical wave. Even if the samples are prepared on the same embryonic day and a similar imaging point in the cochlear epithelium is chosen for the time-lapse experiment, the stage of HC differentiation at the imaging point may differ slightly from sample to sample. Moreover, the laser power of the confocal microscope varies and is different in every time-lapse imaging experiment. The difference can be ignored when the fluorescence of the specimen is strong enough, but the time-lapse experiment using feeble fluorescence is sensitive to the minor change of laser power. The fluorescence of *Atoh1*-EGFP was weak and we modified the imaging condition every time, especially the laser power of confocal microscopy, so as to achieve both lower laser toxicity and higher fluorescent signal. Because of these limitations, it was difficult to make a direct comparison and statistical analyses among time-lapse imaging experiments.

In order to overcome this problem, the standardization of time and fluorescent signal was performed using an algorithm to detect FEP, that is, the first appearance of developing outer hair cells. To quantify the FEP of Atoh1-positive signals in the x-axis, we first generated kymographs of *Atoh1*-EGFP signals by performing maximum projection in the z-axis and averaged projection in the y-axis. As the samples slightly shift during the live imaging, the position of the kymograph was corrected at each time point on the basis of the developing IHC position, automatically detected as a local maximum of signals. The medial edge of GFP expression was regarded as x position 0. We used only the samples established at E14.5 to quantify FEP because the distinct signals of developing IHCs were needed for the accuracy of the automated medial edge detection. Then, we defined the Atoh1-positive signals by binarizing the signal intensity in a threshold manner. In so doing, we employed the mode of intensity over entire live imaging data as the background signal B, and set the threshold value T as $T=nB$, where n is arbitrary value. The background signal was defined as the intensity that was the most frequent value in the whole shooting range of all time frames. Here, we used $n=3.5$; the results do not change qualitatively even if other values were used. Finally, we evaluated when the size of Atoh1-positive signals reaches that of nuclei (~5 µm), and defined the FEP as median of those positions.

Next, we defined the 'medial area' and 'lateral area' based on the time of FEP to quantify the medial-lateral gradient of initial Atoh1 expression in the prosensory domain lateral to developing IHCs. As shown in Fig. 6E, the medial area was where x position was between 10 µm and 25 µm, and the lateral area was where x position was between 25 µm and 40 µm. The average of relative GFP intensity was calculated for 1 h after the time of FEP.

Finally, we performed three-dimensional cell tracking in E14.5 *Atoh1*-EGFP cochlear explants based on the time standardization using FEP, that is, the time of FEP was regarded as zero. The tracking started at 4 h before FEP time in each experiment, using Imaris software (as described above). Some IHCs had already been detected, but no OHCs had yet appeared at 4 h before FEP time. At least three tracks of IHCs in each experiment were used for drift correction so that the position of IHCs was fixed. The time and position of the first spots in OHC tracks were detected, and the distance between average IHC position and the individual first OHC spots was calculated by projection to the xz plane. Data was collected from three experiments in each of these three groups; control experiments, the experiments with 30 µM cyclopamine and the experiments with 50 nM LDN193189. The correlation between the distance and time were estimated using Pearson's correlation coefficient.

Statistical analysis

Three or more experiments from each group were analyzed in all statistical analyses. Data are expressed as mean±s.e.m. Student–Newman–Keuls tests were used to detect differences among groups. Wilcoxon t-tests were used to detect differences between paired groups. Differences at $P<0.05$ were regarded as statistically significant.

Acknowledgements

We thank Dr Mikio Hoshino, Dr Mayumi Yamada and Dr Tomoo Owa for Tg-*Atoh1-Cre* mice and the anti-Atoh1 antibody, and Dr Kosuke Yusa for the pMCS-*DTA* retrieval vector. This work was supported by the Kyoto University Live Imaging Center. We are grateful to Dr Nathan V. Welham for helpful discussions. We also thank Dr Shinya Kuwata and Dr Yusuke Yamaoka for providing assistance in performing experiments.

Competing interests

The authors declare no competing or financial interests.

Author contributions

Conceptualization: T.T., R.K.; Methodology: T.T., S.S., F.I., T.H.; Software: T.H.; Validation: T.T., T.H.; Formal analysis: T.T., T.H.; Investigation: T.T., S.S., F.I.; Resources: I.I.; Data curation: T.T., T.H.; Writing - original draft: T.T., T.H., I.I.; Writing - review & editing: T.T., S.S., F.I., T.H., I.I., R.K.; Visualization: T.T.; Supervision: R.K.; Project administration: T.T., R.K.; Funding acquisition: T.T., I.I., R.K.

Funding

This work was supported by Core Research for Evolutional Science and Technology (CREST) (JPMJCR12W2, R.K.); Grant-in-Aid for Scientific Research on Innovative Areas (16H06480, R.K.) and Scientific Research (C) (25462635, T.T.) from the Ministry of Education, Culture, Sports, Science, and Technology (MEXT), Japan; The Program for Technological Innovation of Regenerative Medicine (JP18bm0704020, I.I.) from the Japan Agency for Medical Research and Development and the Takeda Medical Research Foundation (T.T.).

Supplementary information

Supplementary information available online at
http://dev.biologists.org/lookup/doi/10.1242/dev.177881.supplemental

References

Abdolazimi, Y., Stojanova, Z. and Segil, N. (2016). Selection of cell fate in the organ of Corti involves the integration of Hes/Hey signaling at the Atoh1 promoter. *Development* **143**, 841-850. doi:10.1242/dev.129320

Abe, T., Kiyonari, H., Shioi, G., Inoue, K.-I., Nakao, K., Aizawa, S. and Fujimori, T. (2011). Establishment of conditional reporter mouse lines at ROSA26 locus for live cell imaging. *Genesis* **49**, 579-590. doi:10.1002/dvg.20753

Ahmed, M., Wong, E. Y. M., Sun, J., Xu, J., Wang, F. and Xu, P.-X. (2012). Eya1-Six1 interaction is sufficient to induce hair cell fate in the cochlea by activating Atoh1 expression in cooperation with Sox2. *Dev. Cell* **22**, 377-390. doi:10.1016/j.devcel.2011.12.006

Anniko, M. (1983). Cytodifferentiation of cochlear hair cells. *Am. J. Otolaryngol.* **4**, 375-388. doi:10.1016/S0196-0709(83)80043-X

Bermingham, N. A., Hassan, B. A., Price, S. D., Vollrath, M. A., Ben-Arie, N., Eatock, R. A., Bellen, H. J., Lysakowski, A. and Zoghbi H. Y. (1999). Math1: an essential gene for the generation of inner ear hair cells. *Science* **284**, 1837-1841. doi:10.1126/science.284.5421.1837

Bok, J., Zenczak, C., Hwang, C. H. and Wu, D. K. (2013). Auditory ganglion source of Sonic hedgehog regulates timing of cell cycle exit and differentiation of mammalian cochlear hair cells. *Proc. Natl. Acad. Sci. USA* **110**, 13869-13874. doi:10.1073/pnas.1222341110

Cai, T., Seymour, M. L., Zhang, H., Pereira, F. A. and Groves, A. K. (2013). Conditional deletion of Atoh1 reveals distinct critical periods for survival and function of hair cells in the organ of Corti. *J. Neurosci.* **33**, 10110-10122. doi:10.1523/JNEUROSCI.5606-12.2013

Chen, P., Johnson, J. E., Zoghbi, H. Y. and Segil, N. (2002). The role of Math1 in inner ear development: Uncoupling the establishment of the sensory primordium from hair cell fate determination. *Development.* **29**, 2495-2505. doi:10.3410/f.1006295.78812

Fujiyama, T., Yamada, M., Terao, M., Terashima, T., Hioki, H., Inoue, Y. U., Inoue, T., Masuyama, N., Obata, K., Yanagawa, Y. et al. (2009). Inhibitory and excitatory subtypes of cochlear nucleus neurons are defined by distinct bHLH transcription factors, Ptf1a and Atoh1. *Development* **136**, 2049-2058. doi:10.1242/dev.033480

Hayashi, T., Cunningham, D. and Bermingham-McDonogh, O. (2007). Loss of Fgfr3 leads to excess hair cell development in the mouse organ of Corti. *Dev Dyn.* **236**, 525-533. doi:10.1002/dvdy.21026

Hayashi, T., Kokubo, H., Hartman, B. H., Ray, C. A., Reh, T. A. and Bermingham-McDonogh, O. (2008). Hesr1 and Hesr2 may act as early effectors of Notch signaling in the developing cochlea. *Dev. Biol.* **316**, 87-99. doi:10.1016/j.ydbio.2008.01.006

Helms, A. H., Abney, A. H., Ben-Arie, N., Zoghbi, H. Y. and Johnson, J. E. (2000). Autoregulation and multiple enhancers control Math1 expression in the developing nervous system. *Development* **127**, 1185-1196.

Imayoshi, I., Shimogori, T., Ohtsuka, T. and Kageyama, R. (2008). Hes genes and neurogenin regulate non-neural versus neural fate specification in the dorsal telencephalic midline. *Development* **135**, 2531-2541. doi:10.1242/dev.021535

Imayoshi, I., Hirano, K., Sakamoto, M., Miyoshi, G., Imura, T., Kitano, S., Miyachi, H. and Kageyama, R. (2012). A multifunctional teal-fluorescent Rosa26 reporter mouse line for Cre- and Flp-mediated recombination. *Neurosci. Res.* **73**, 85-91. doi:10.1016/j.neures.2012.02.003

Imayoshi, I., Isomura, A., Harima, Y., Kawaguchi, K., Kori, H., Miyachi, H., Fujiwara, T., Ishidate, F. and Kageyama, R. (2013). Oscillatory control of factors determining multipotency and fate in mouse neural progenitors. *Science* **342**, 1203-1208. doi:10.1126/science.1242366

Jacques, B. E., Montcouquiol, M. E., Layman, E. M., Lewandoski, M. and Kelley, M. W. (2007). Fgf8 induces pillar cell fate and regulates cellular patterning in the mammalian cochlea. *Development* **134**, 3021-3029. doi:10.1242/dev.02874

Jones, S. M. and Jones, T. M. (2011). *Genetics, Embryology and Development of Auditory and Vestibular Systems*. Plural Publishing.

Kageyama, R., Ohtsuka, T. and Kobayashi, T. (2007). The Hes gene family: repressors and oscillators that orchestrate embryogenesis. *Development* **134**, 1243-1251. doi:10.1242/dev.000786

Kanki, H., Suzuki, H. and Itohara, S. (2006). High-efficiency CAG-FLPe delete mice in C57BL/6J background. *Exp. Anim.* **55**, 137-141. doi:10.1538/expanim.55.137

Kelley, M. W. (2007). Cellular commitment and differentiation in the organ of Corti. *Int. J. Dev. Biol.* **51**, 571-583. doi:10.1387/ijdb.072388mk

Kelly, M. C. and Chen, P. (2009). Development of form and function in the mammalian cochlea. *Curr. Opin. Neurobiol.* **19**, 395-401. doi:10.1016/j.conb.2009.07.010

Kiernan, A. E., Cordes, R., Kopan, R., Gossler, A. and Gridley, T. (2005). The Notch Ligands DLL1 and JAG2 act synergistically to regulate hair cell development in the mammalian inner ear. *Development* **132**, 4353-4362. doi:10.1242/dev.02002

Ladhams, A. and Pickles, J. O. (1996). Morphology of the monotreme organ of Corti and macula lagena. *J. Comp. Neurol.* **366**, 335-347. doi:10.1002/(SICI)1096-9861(19960304)366:2<335::AID-CNE11>3.0.CO;2-O

Lanford, P. J., Lan, Y., Jiang, R., Lindsell, C., Weinmaster, G., Gridley, T. and Kelley, M. W. (1999). Notch signalling pathway mediates hair cell development in mammalian cochlea. *Nat. Genet.* **21**, 289-292. doi:10.1038/6804

Lanford, P. J., Shailam, R., Norton, C. R., Ridley, T. and Kelley, M. W. (2000). Expression of Math1 and HES5 in the cochleae of wildtype and Jag2 mutant mice. *J. Assoc. Res. Otolaryngol.* **1**, 161-171. doi:10.1007/s101620010023

Lee, E.-C., Yu, D., Martinez de Velasco, J., Tessarollo, L., Swing, D. A., Court, D. L., Jenkins, N. A. and Copeland, N. G. (2001). A highly efficient Escherichia coli-based chromosome engineering system adapted for recombinogenic targeting and subcloning of BAC DNA. *Genomics* **73**, 56-65. doi:10.1006/geno.2000.6451

Li, S., Mark, S., Radde-Gallwitz, K., Schlisner, R., Chin, M. T. and Chen, P. (2008). Hey2 functions in parallel with Hes1 and Hes5 for mammalian auditory sensory organ development. *BMC Dev. Biol.* **8**, 20. doi:10.1186/1471-213X-8-20

Lumpkin, E. A., Collisson, T., Parab, P., Omer-Abdalla, A., Haeberle, H., Chen, P., Doetzlhofer, A., White, P., Groves, A., Segil, N. et al. (2003). Math1-driven GFP expression in the developing nervous system of transgenic mice. *Gene Expr. Patterns* **3**, 389-395. doi:10.1016/S1567-133X(03)00089-9

Manley, G. A. and Köppl, C. (1998). Phylogenetic development of the cochlea and its innervation. *Curr. Opin. Neurobiol.* **8**, 468-474. doi:10.1016/S0959-4388(98)80033-0

Morrison, A., Hodgetts, C., Gossler, A., Hrabé de Angelis, M. and Lewis, J. (1999). Expression of Delta1 and Serrate1 (Jagged1) in the mouse inner ear. *Mech. Dev.* **84**, 169-172. doi:10.1016/S0925-4773(99)00066-0

Munnamalai, V. and Fekete, D. M. (2016). Notch-Wnt-Bmp crosstalk regulates radial patterning in the mouse cochlea in a spatiotemporal manner. *Development* **143**, 4003-4015. doi:10.1242/dev.139469

Ohyama, T., Basch, M. L., Mishina, Y., Lyons, K. M. Segil, N. and Groves, A. K. (2010). BMP signaling is necessary for patterning the sensory and nonsensory regions of the developing mammalian cochlea. *J. Neurosci.* **30**, 15044-15051. doi:10.1523/JNEUROSCI.3547-10.2010

Puligilla, C., Feng, F., Ishikawa, K., Bertuzzi, S., Dabdoub, A., Griffith, A. J., Fritzsch, B. and Kelley, M. W. (2007). Disruption of fibroblast growth factor receptor 3 signaling results in defects in cellular differentiation, neuronal patterning, and hearing impairment. *Dev. Dyn.* **236**, 1905-1917. doi:10.1002/dvdy.21192

Raft, S., Koundakjian, E. J., Quinones, H., Jayasena, C. S., Goodrich, L. V., Johnson, J. E., Segil, N. and Groves, A. K. (2007). Cross-regulation of Ngn1 and Math1 coordinates the production of neurons and sensory hair cells during inner ear development. *Development* **134**, 4405-4415. doi:10.1242/dev.009118

Rose, M. F., Ren, J., Ahmad, K. A., Chao, H.-T., Klisch, T. J., Flora, A., Greer, J. J. and Zoghbi, H. Y. (2009). Math1 is essential for the development of hindbrain neurons critical for perinatal breathing. *Neuron* **64**, 341-354. doi:10.1016/j.neuron.2009.10.023

Rubel, E. W. (1978). Ontogeny of structure and function in the vertebrate auditory system. In *Handbook of Sensory Physiology*, Vol. IX (ed. M. Jacobson), pp. 135-237. New York: Springer.

Shim, K., Minowada, G., Coling, D. E. and Martin, G. R. (2005). Sprouty2, a mouse deafness gene, regulates cell fate decisions in the auditory sensory epithelium by antagonizing FGF signaling. *Dev. Cell* **8**, 553-564. doi:10.1016/j.devcel.2005.02.009

Tateya, T., Imayoshi, I., Tateya, I., Ito, J. and Kageyama, R. (2011). Cooperative functions of Hes/Hey genes in auditory hair cell and supporting cell development. *Dev. Biol.* **352**, 329-340. doi:10.1016/j.ydbio.2011.01.038

Tateya, T., Imayoshi, I., Tateya, I., Hamaguchi, K., Torii, H., Ito, J. and Kageyama, R. (2013). Hedgehog signaling regulates prosensory cell properties during the basal-to-apical wave of hair cell differentiation in the mammalian cochlea. *Development* **140**, 3848-3857. doi:10.1242/dev.095398

Wan, G., Corfas, G. and Stone, J. S. (2013). Inner ear supporting cells: rethinking the silent majority. *Semin. Cell Dev. Biol.* **24**, 448-459. doi:10.1016/j.semcdb.2013.03.009

Warming, S., Costantino, N., Court, D. L., Jenkins, N. A. and Copeland, N. G. (2005). Simple and highly efficient BAC recombineering using galK selection. *Nucleic Acids Res.* **33**, e36. doi:10.1093/nar/gni035

Woods, C., Montcouquiol, M. and Kelley, M. W. (2004). Math1 regulates development of the sensory epithelium in the mammalian cochlea. *Nat. Neurosci.* **12**, 1310-1318. doi:10.1038/nn1349

Yamada, M., Seto, Y., Taya, S., Owa, T., Inoue, Y. U., Inoue, T., Kawaguchi, Y., Nabeshima, Y. and Hoshino, M. (2014). Specification of spatial identities of cerebellar neuron progenitors by ptf1a and atoh1 for proper production of GABAergic and glutamatergic neurons. *J. Neurosci.* **34**, 4786-4800. doi:10.1523/JNEUROSCI.2722-13.2014

Yamamoto, N., Okano, T., Ma, X., Adelstein, R. S. and Kelley, M. W. (2009). Myosin II regulates extension, growth and patterning in the mammalian cochlear duct. *Development* **136**, 1977-1986. doi:10.1242/dev.030718

Zheng, J. L. and Gao, W.-Q. (2000). Overexpression of math1 induces robust production of extra hair cells in postnatal rat inner ears. *Nat. Neurosci.* **3**, 580-586. doi:10.1038/75753

Zine, A., Aubert, A., Qiu, J., Therianos, S., Guillemot, F., Kageyama, R. and de Ribaupierre, F. (2001). Hes1 and Hes5 activities are required for the normal development of the hair cells in the mammalian inner ear. *J. Neurosci.* **21**, 4712-4720. doi:10.1523/JNEUROSCI.21-13-04712.2001

Supplementary Data

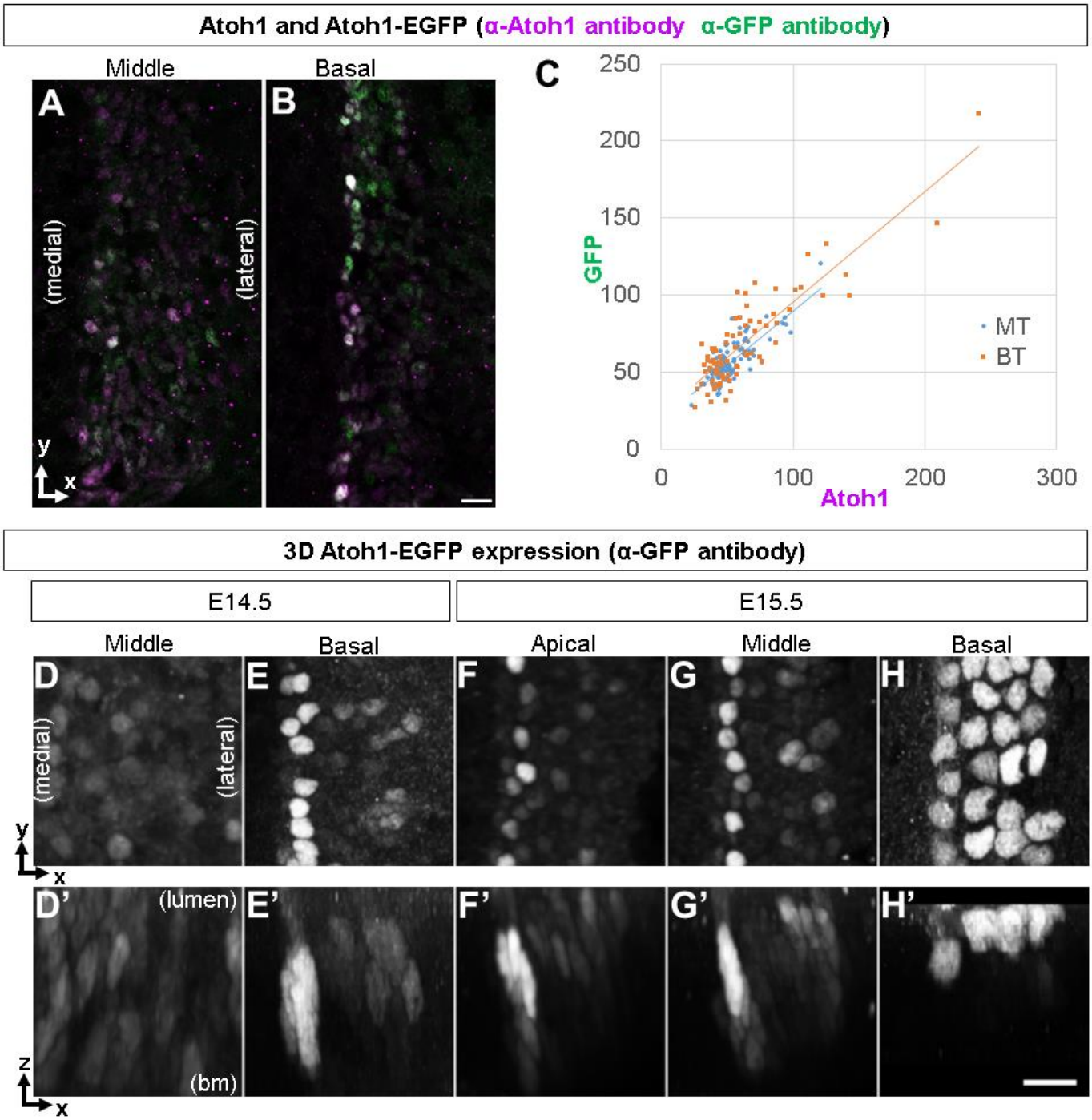

Fig. S1. GFP intensity in prosensory cells of cochleae of *Atoh1*-EGFP mouse embryos can be interpreted as representative of endogenous Atoh1 levels.

(A-C) Comparison of *Atoh1*-EGFP with endogenous Atoh1 expression.

We carried out an immunohistochemical analysis of *Atoh1*-EGFP in the cochlear epithelium of E14.5 embryos using both anti-GFP and anti-Atoh1 antibodies.

(A, B) Atoh1 and GFP expression in the middle turn (A) and basal turn (B) of E14.5 *Atoh1*-EGFP cochlear epithelium visualized by anti-GFP (green) and anti-Atoh1 (magenta) antibody. In prosensory cells, weak, diffuse and salt-and-pepper staining was detected by both anti-GFP and anti-Atoh1 antibodies.

Scale bar: a and b, 10 μm.

(C) Relative expression intensity of Atoh1 and GFP in individual GFP-positive cells of E14.5 *Atoh1*-EGFP cochlear epithelium. A significant positive linear correlation was observed between relative GFP intensity and relative Atoh1 intensity (MT, $r = 0.787$; BT, $r = 0.877$, $p < 0.01$). MT, middle turn; BT, basal turn. Blue or orange dots indicate MT or BT cells, respectively. The linear approximation curves of MT (blue) and BT (organe) were also shown in the graph.

(D-H) Two-dimensional xy and xz projection images of *Atoh1*-EGFP expression in the developing cochlear epithelium visualized by anti-GFP antibody (grayscale).

It is important to detect low levels of Atoh1 in the xz plane as these are thought to change drastically along this plane from the prosensory domain, a pseudostratified epithelium about five cells thick, into the organ of Corti, two cells thick with HC nuclei on its luminal side and SC nuclei on its basement membrane side. Therefore, two-dimensional xz projection images, as well as two-dimensional xy projection images, were recomposed using confocal z-stack images obtained from whole-mounted, surface-prepared cochlear specimens.

(D-H) xy optical projections. (D'-H') xz single-plane confocal images.

(D, D') E14.5 middle turn. GFP expression was weak and diffuse in the middle turn, and had no gradation along the x-axis or z-axis.

(E, E') E14.5 basal turn. (F, F') E15.5 apical turn. A high level of GFP was observed in cells located at the most medial edge of the GFP-positive area (E, E', F, F').

(G, G') E15.5 middle turn. GFP expression increased in the cells of the lateral prosensory compartment, not only near the luminal side but also near the basement membrane side, along the z-axis.

(H, H') E15.5 basal turn. Strong GFP signals were restricted to cells located near the lumen that were arranged in four rows, suggesting that these GFP-positive cells were differentiating HCs.

bm, basement membrane. Scale bar: D - H', 10 μm.

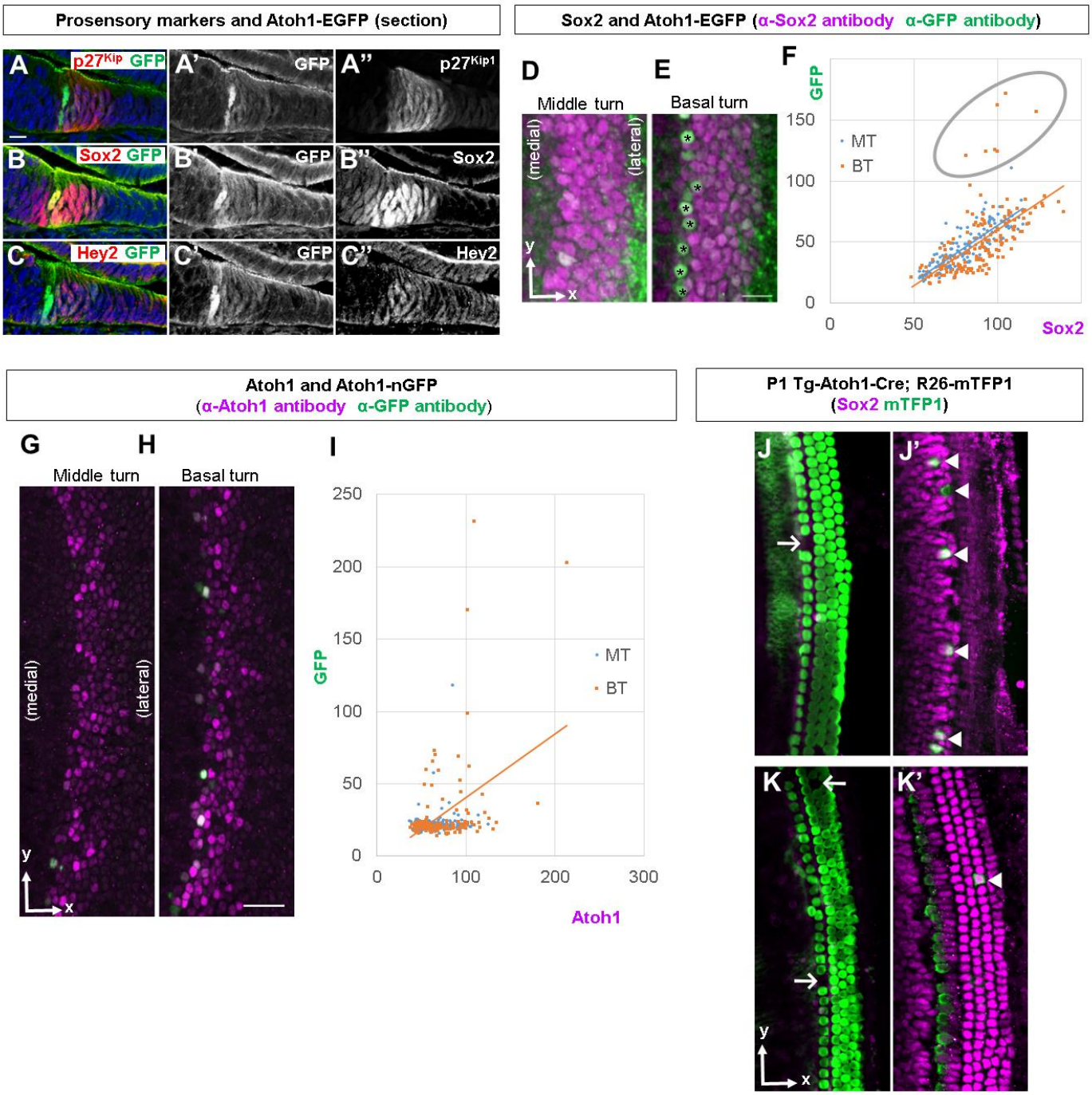

Fig. S2. Atoh1 expression in the developing cochlear epithelium.

(A-C) Weak Atoh1 expression in the prosensory domain.

Immunohistochemical staining for GFP and the prosensory markers p27Kip1, Sox2 and Hey2 in Phase II (E14.5 basal turn) of *Atoh1*-EGFP cochlear mid-modiolar sections.

(A-C) GFP (green), other prosensory markers p27Kip1, Sox2 or Hey2 (magenta), and DAPI (blue).

(A'-C') GFP in gray scale.

(A"-C") p27Kip1, Sox2 and Hey2 prosensory markers in gray scale. Scale bar: A-C, A'-C', A"-C", 10 μm.

(D-F) Weak Atoh1 expression in Phases I and II is correlated with Sox2 expression levels.

GFP and Sox2 expression in E14.5 *Atoh1*-EGFP whole cochlear epithelium visualized by anti-GFP antibody (green) and anti-Sox2 antibody (magenta).

(D) E14.5 middle turn of *Atoh1*-EGFP cochlea, corresponding to phase I. GFP tended to be expressed in the cells that expressed Sox2 more intensely.

(E) E14.5 basal turn of *Atoh1*-EGFP cochlea, corresponding to Phase II. A similar association to that seen in Phase I was observed. Asterisks indicate the cells that express high GFP. Scale bar: D and E, 10 μm.

(F) Relative intensity of Sox2 and GFP in individual cells. MT, middle turn (blue) ; BT, basal turn (orange). A significant positive linear correlation was observed between Sox2 and GFP (MT, $r = 0.828$; BT, $r = 0.607$, $p<0.01$). The linear approximation curves of MT (blue) and BT (orange) were shown in the graph.

The seven points circled with gray lines are the cells indicated in panel E by asterisks, and are outliers from the linear approximation curve as their relative increase in Sox2 was less than that of GFP.

(G-K, J'-K') Atoh1 enhancer becomes active in cells fated to be hair cells, not in the prosensory cells before fate determination.

(G-I) Comparison of *Atoh1*-nGFP reporter with endogenous Atoh1 expression in E14.5 cochlear epithelium.

(G, H) GFP expression in E14.5 cochlear epithelium of *Atoh1*-nGFP mice was compared with endogenous Atoh1 expression by immunohistochemistry, using anti-GFP (green) and anti-Atoh1 (magenta) antibodies. (G) Middle turn corresponding to Phase I. (H) Basal turn corresponding to Phase II. Scale bar: G and H, 20 μm.

(I) Relative intensity of Atoh1 and GFP in individual cells are plotted as blue dots (middle turn, also shown in panel G) and orange dots (basal turn, also shown in panel H). There is a significant positive linear correlation between Atoh1 and GFP of cells in the basal turn (BT) ($r = 0.411$, $p < 0.01$), but a positive linear correlation was not observed in the middle turn (MT) ($r = 0.147$). The linear approximation curves of BT (orange) was shown in the graph.

(J-K, J'-K') Cell lineage detected after Atoh1 enhancer activity. Tg-*Atoh1*-Cre mice, in which the Cre expression is driven by an Atoh1 enhancer element, were crossed with R26-mTFP1 reporter mice so as to detect cell lineage of the same populations labeled by GFP in *Atoh1*-nGFP mice. Double transgenic offspring were harvested at postnatal day 1 and analyzed using antibodies against mTFP (green) and Sox2 (magenta). mTFP1 was detected using an anti-HA antibody.

(J, K) Single plane confocal images in which rows of HC nuclei are apparent. Most HCs stained positively for mTFP1, but mTFP1-negative HCs were occasionally seen (arrows).

(J', K') Single plane confocal images in which rows of Sox2-positive SC nuclei are apparent at the same x-y position as panels J and K. Sox2-positive SCs were mostly mTFP1-negative but some were mTFP1-positive (arrowheads).

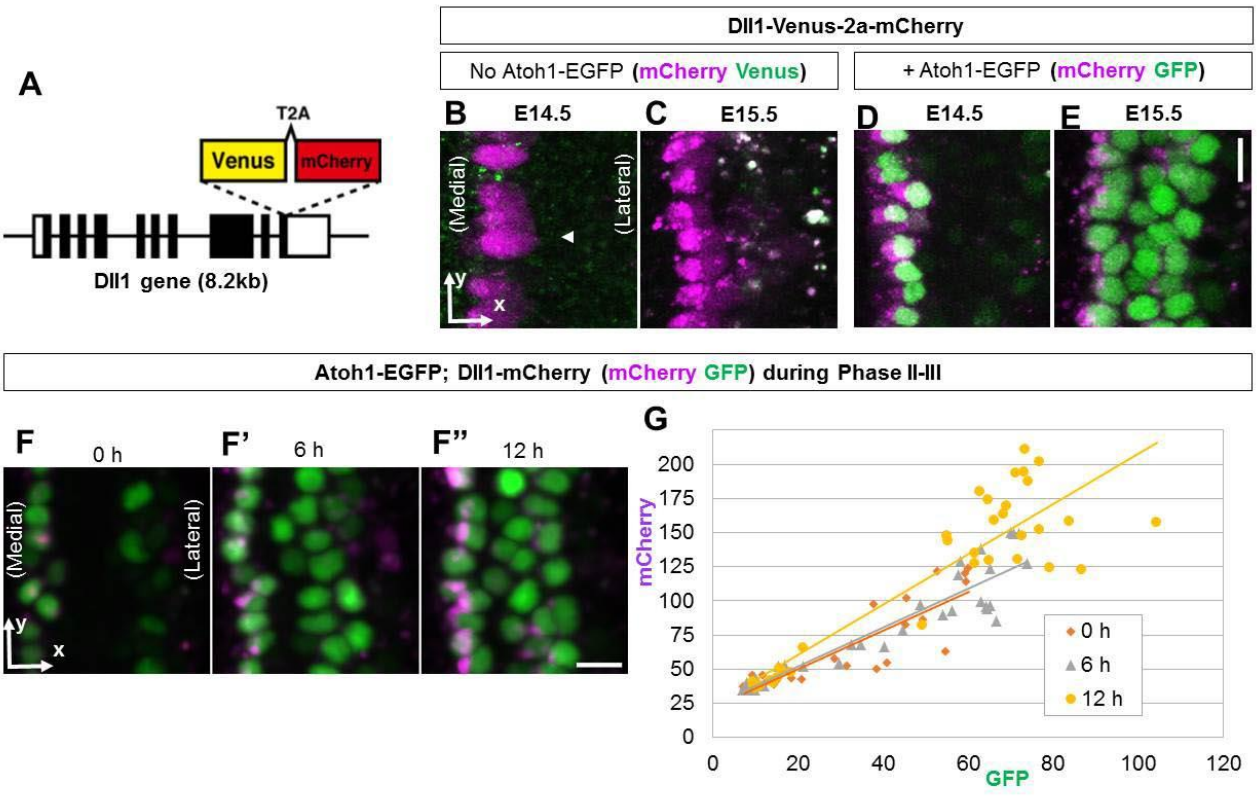

Fig. S3. Visualization of hair cell fate determination using Dll1 C-terminal Venus-T2A-mCherry.

(A) Dll1 C-terminal Venus-T2A-mCherry fusion reporter knock-in construct.

(B-E) GFP imaging is not affected by Venus fluorescence in the double transgenic mice of *Atoh1*-EGFP and Dll1-Venus-2a-mCherry.

Dll1-Venus-T2A-mCherry cochlear explants were analyzed using live imaging; the detection of GFP was not affected by Venus fluorescence in the double transgenic mice carrying *Atoh1*-EGFP and Dll1-Venus-T2A-mCherry.

(B, C) Live imaging of Dll1-Venus-T2A-mCherry cochlear epithelium.

(B) E14.5 basal turn, corresponding to Phase II. mCherry (magenta) was detected in a row of presumptive IHCs. There was little Venus signal (green) in the imaging conditions for GFP detection.

(C) E15.5 basal turn, corresponding to Phase III. mCherry (magenta) was weakly expressed in the lateral compartment. There was little Venus signal (green) in the imaging conditions for GFP detection.

(D, E) Live imaging of Dll1-Venus-T2A-mCherry; *Atoh1*-EGFP cochlear epithelium. The signal of mCherry was derived from Dll1-Venus-T2A-mCherry, and the signal of GFP was thought to be derived from *Atoh1*-EGFP.

(D) E14.5 basal turn. (E) E15.5 basal turn.

(F-F", G) Dll1 is expressed in *Atoh1*-high cells during Phase II-III in *Atoh1*-EGFP;Dll1-mCherry cochlear epithelium.

Atoh1-EGFP; Dll1-mCherry cochlear explants were established at E14.5 and time-lapse imaging was performed.

(F-F”) Two-dimensional xy projection images at 0 h (F), 6 h (F’) and 12 h (F”) from the start of imaging, indicating the transition from Phase II to Phase III.

(G) Relative GFP and mCherry intensity in individual cells.

The number of cells expressing both high GFP and mCherry increased with time. A significant positive linear correlation between Atoh1 and mCherry was observed at all three time points (0 h, $r = 0.893$; 6 h, $r = 0.927$; 12 h, $r = 0.895$, $p < 0.01$), and the linear approximation curves at each time point shown in the graph were similar.

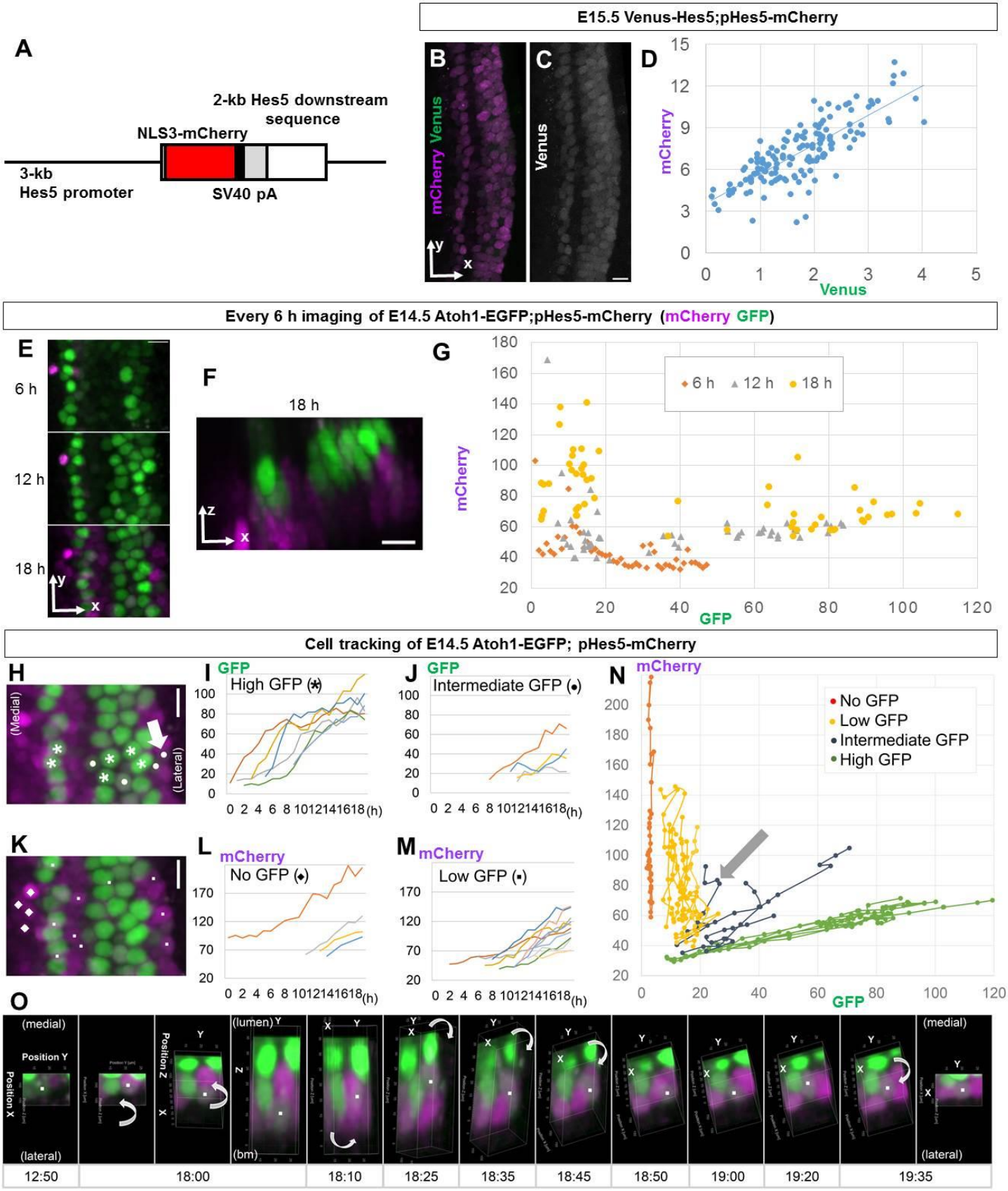

Fig. S4. Live imaging of *Hes5* in the developing cochlear epithelium.

(A-G) Visualization of supporting cell fate determination by pHes5-mCherry line.

(A) pHes5-NLS3-mCherry reporter construct.

(B-D) mCherry expression of pHes5-mCherry cochleae mimics endogenous Hes5 expression.

As immunolabeling for Hes5 was difficult, pHes5-NLS3-mCherry mice were crossed with Venus-Hes5 fusion knock-in mice, in which Venus expression faithfully represents endogenous Hes5 expression (Imayoshi et al., 2013).

(B,C) E15.5 pHes5-mCherry;Venus-Hes5 cochlear epithelium, corresponding to Phase III, expressed both mCherry (magenta in B) and Venus (green in B and grayscale in C), though Venus signal intensity was faint. The fluorescence of mCherry and Venus was captured by confocal microscopy. mCherry expression in the cochlea of pHes5-mCherry embryos mimicked endogenous Hes5 expression and was more readily detectable.

(D) The relative intensity of mCherry and Venus in individual cells. A significant positive linear correlation was observed ($r = 0.788$, $p < 0.01$).

(E-G) Most prosensory cells become either Atoh1-dominant cells or Hes5-dominant cells.

Atoh1-EGFP;pHes5-mCherry cochlear explants were established at E14.5 and time-lapse imaging was performed.

(E) Two-dimensional xy projection images at 6, 12 and 18 h after the start of imaging, covering the transition period from Phase II to Phase III. (F) A snapshot of xz projection (the same view as **Movie 6**) at 18 h. (G) The relative intensity of GFP and mCherry within individual cells. At 6 h, most cells showed low GFP/low mCherry levels; thereafter, two subpopulations of high GFP/low mCherry and low GFP/high mCherry gradually appeared over time. This suggests that most prosensory cells become either Atoh1-dominant cells or Hes5-dominant cells.

(H-O) Cell tracking of *Atoh1*-EGFP;pHes5-mCherry during Phases II-III reveals that neutral cells express intermediate levels of Atoh1 and Hes5 at the end of Phase III

Cells that expressed GFP and/or mCherry in cochlear explants of *Atoh1*-EGFP;pHes5-mCherry embryos at E14.5 were tracked to the end of the experiment at 19 hours, and found to fall into four groups according to GFP intensity: high GFP, intermediate GFP, low GFP and no GFP.

(H) xy projection images at 19 h. GFP (green) and mCherry (magenta). Six cells exhibited high GFP (asterisks), and 4 cells exhibited intermediate GFP (dots). (I) Relative GFP intensity of high GFP cells per hour. As time progressed, the GFP intensity of cells with high GFP levels increased. It indicated that cells with high GFP were committed to an HC fate. (J) Relative GFP intensity of intermediate GFP cells per hour. (K) xy projection images at 19 h. GFP (green) and mCherry (magenta). Ten cells exhibited low GFP (small dots), and four cells exhibited no-GFP (rhombuses). (L) Relative mCherry intensity of no GFP cells per hour. (M) Relative mCherry intensity of low GFP cells per hour. The mCherry intensity of cells with no GFP or low GFP increased. Cells with no or low GFP were thought to be committed to an SC fate. (N) GFP and mCherry intensities of individual tracks. A subpopulation of intermediate GFP cells (blue) were located between two cell subpopulations with high GFP/low mCherry cells (green) and low GFP/high mCherry cells (yellow). This observation suggests that cells with an intermediate GFP level may be “neutral”, and that their fate commitment remains undetermined. **Movies 7 and 8** show a representative neutral cell that corresponds to those arrowed in H, N.

(O) A series of snapshots of **Movie 8**. Arrows indicate the direction to rotate the image. The marked cell is the same as indicated by arrows in H and N, and adjacent to a cell with a high GFP level and a cell with high mCherry level and moves up and down in **Movie 8**.

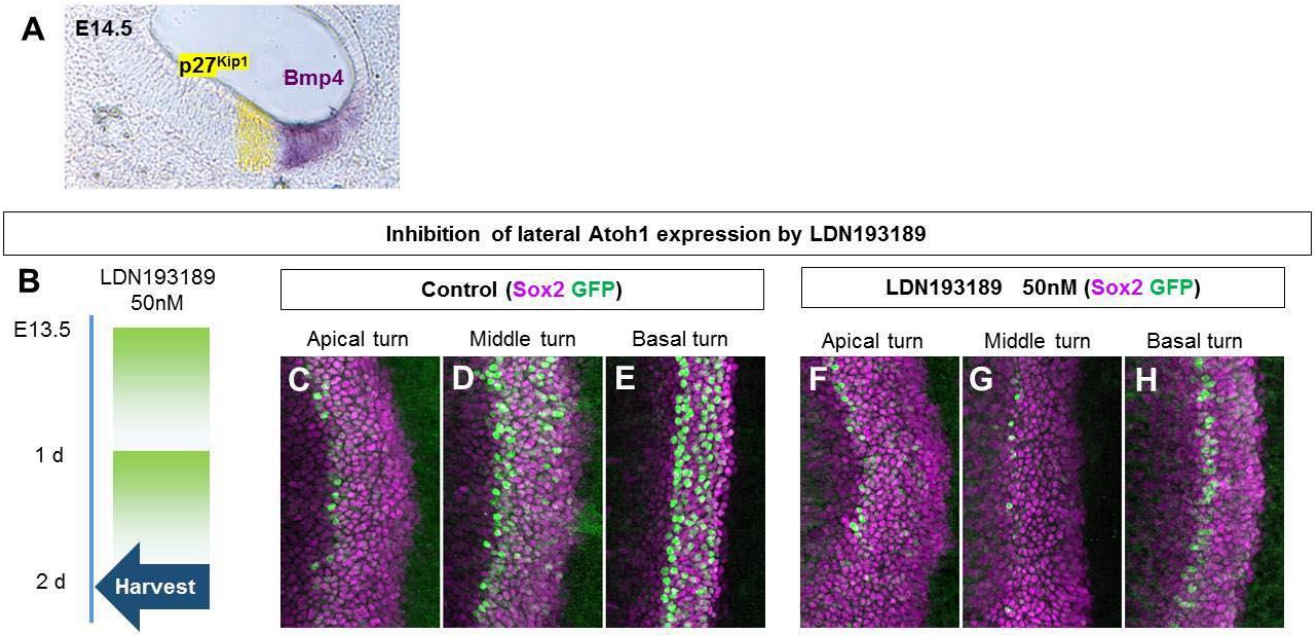

Fig. S5. The effects of Bmp signaling on OHC differentiation.

(A) Bmp4 is expressed in the cochlear epithelium lateral to the prosensory domain.

In situ hybridization of Bmp4 in E14.5 cochlear mid-modiolar sections. Bmp4 is expressed in the cochlear epithelium lateral to p27Kip1-positive prosensory domain.

(B-H) OHC differentiation is suppressed by a Bmp4 signaling inhibitor.

The Bmp4 inhibitor LDN193189 was used to elucidate the Bmp4 signaling pathway in prosensory cells.

(B) The schedule for explant culture establishment, inhibitor LDN193189 administration, and sampling.

(C-H) xy projection images obtained using confocal microscopy. E13.5 *Atoh1*-EGFP cochleae were cultured for 2 days with or without LDN193189, harvested, fixed and used immunohistochemically stained for GFP (green) and Sox2 (magenta).

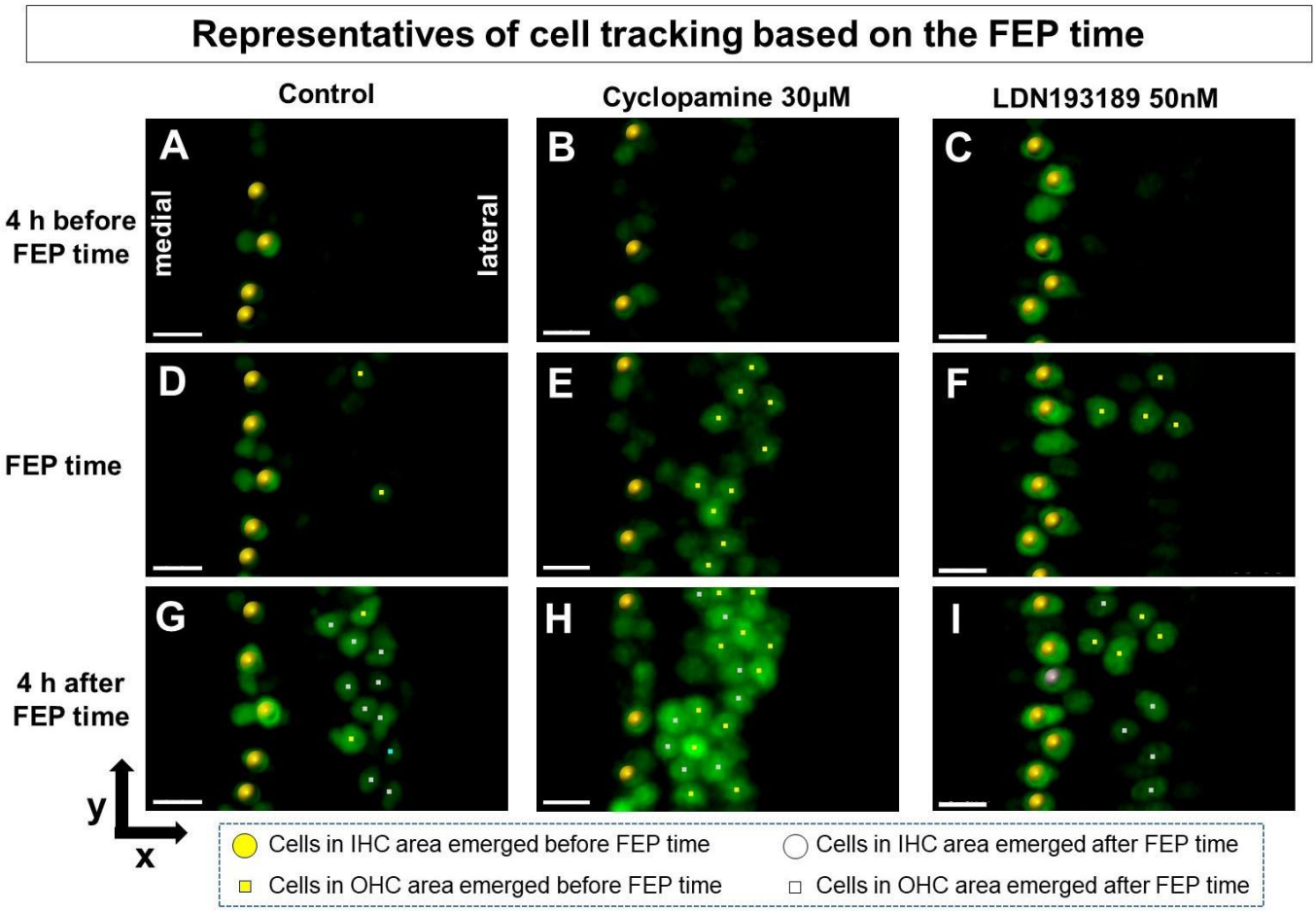

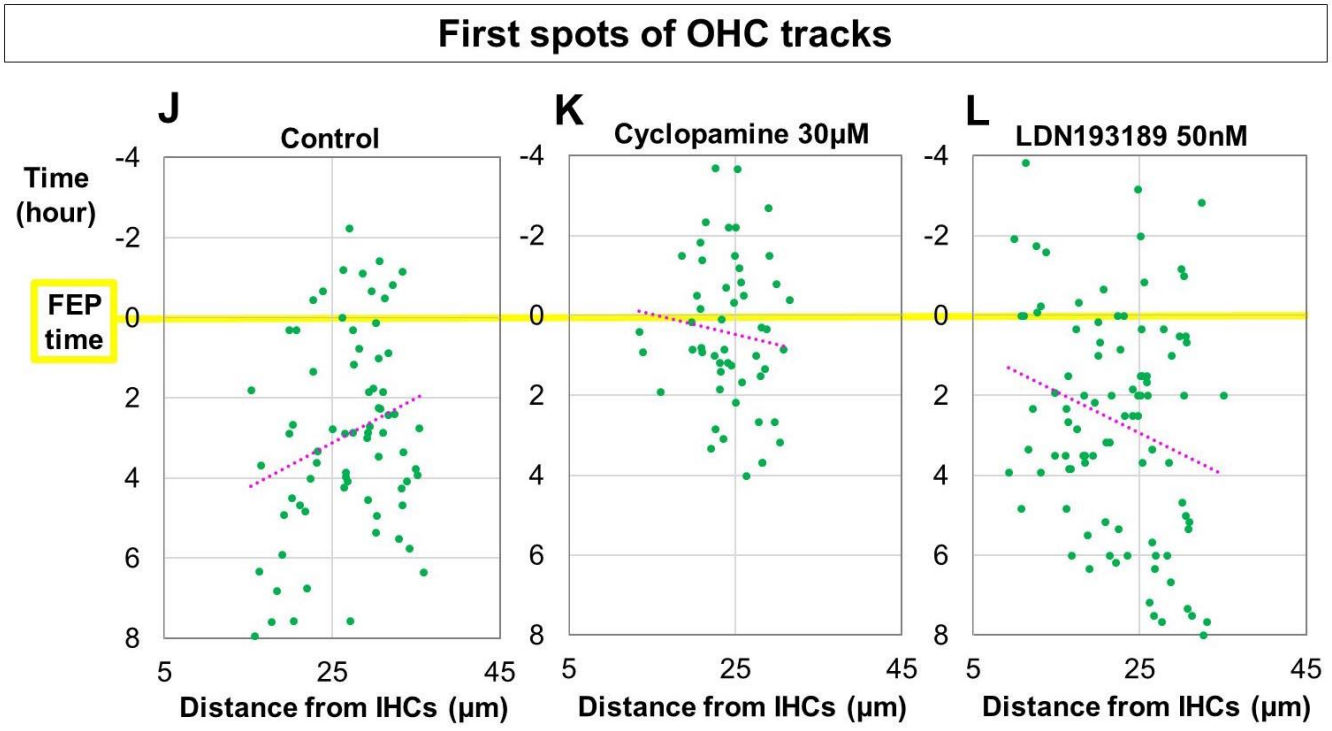

Fig. S6. Effects of Hh inhibitor and Bmp4 inhibitor on Atoh1 expression and OHC patterning.

(A-I) Snapshots of live imaging with Hh inhibitor and Bmp4 inhibitor.

xy projection images of GFP-positive cells in the *Atoh1*-EGFP cochlear explant were tracked from four hours

before the time of FEP. Spheres and squares indicate the cells differentiating into IHCs and OHCs, respectively, and the tracks appeared before the time of FEP are marked by yellow, and those after the time of FEP are white.

(A, D, G) A representative of control experiment. These are the snapshots of **Movie 13**.

(B, E, H) A representative of the experiment with cyclopamine. These are the snapshots of **Movie 14**.

(C, F, I) A representative of the experiment with LDN193189. These are the snapshots of **Movie 15**.

(J-L) The first spots of OHC tracks

Distance between the first spot of each OHC track and mean position of IHCs is calculated, and the distance from IHCs and the time of first OHC spots are plotted. Each of control, cyclopamine and LND193189 group consisted of three time-lapse experiments. A yellow line indicates the time of FEP, and magenta dotted lines are linear approximation curves.

Table S1

Time-lapse imaging conditions

Embryonic day	GFP reporter line	mCherry reporter line	Medicine	Microscope	Total Imaging Time	Time interval (min)	Z-Stack slices	Image size Z (µm)	Scaling Z (µm)	Laser 561nm (%)	Laser 488nm (%)
E14.5	Atoh1-EGFP	Dll1-mCherry	None	LSM780	19h25m	5	25	37.11	1.484	0.1	0.04
E14.5	Atoh1-EGFP	Dll1-mCherry	None	LSM710	20h45m	5	10	42.26	4.700	0.04	0.08
E14.5	Atoh1-EGFP	Dll1-mCherry	None	LSM780	20h50m	5	29	41.56	1.480	0.04	0.1
E14.5	Atoh1-EGFP	pHes5-mCherry	None	LSM780	19h35m	5	27	40.08	1.484	0.02	0.05
E14.5	Atoh1-EGFP	pHes5-mCherry	None	LSM780	22h4m	5	27	40.08	1.484	0.02	0.05
E14.5	Atoh1-EGFP	pHes5-mCherry	None	LSM780	24h54m	5	27	40.08	1.484	0.02	0.05
E13.5	Atoh1-EGFP	R26-H2B-mCherry	None	LSM780	20h0m	5	20	38.66	1.933	0.06	0.5
E14.5	Atoh1-EGFP	pHes5-mCherry	None	LSM780	26h53m	10	6.45	44.4	1.138	0.15	0.04
E13.5	Atoh1-EGFP	pHes5-mCherry	Cyclopamine 30uM	LSM780	45h9m	5	25	31.65	1.266	0.07	0.07
E14.5	Atoh1-EGFP	Dll1-mCherry	Cyclopamine 30uM	LSM710	23h12m	6	28	42.2	1.507	0.07	0.04
E14.5	Atoh1-EGFP	Dll1-mCherry	Cyclopamine 30uM	LSM780	24h10m	5	28	38.84	1.439	0.1	0.05
E14.5	Atoh1-EGFP	Dll1-mCherry	Cyclopamine 30uM	LSM880	20h50m	5	28	40.2	1.489	0.09	0.3
E14.5	Atoh1-EGFP	Dll1-mCherry	Cyclopamine 30uM	LSM880	20h50m	5	26	37.19	1.488	0.09	0.3
E14.5	Atoh1-EGFP	pHes5-mCherry	Cyclopamine 30uM	LSM780	19h20m	10	30	40.89	1.410	0.08	0.02
E14.5	Atoh1-EGFP	pHes5-mCherry	Cyclopamine 30uM	LSM880	47h50m	10	37	43.2	1.200	0.06	0.018
E13.5	Atoh1-EGFP	pHes5-mCherry	LDN 50nM	LSM880	17h9m	5	25	34.47	1.379	0.1	0.2
E14.5	Atoh1-EGFP	Dll1-mCherry	LDN 50nM	LSM780	41h30m	5	28	40.18	1.488	0.1	0.05
E14.5	Atoh1-EGFP	Dll1-mCherry	LDN 50nM	LSM780	44h50m	5	27	37.04	1.425	0.09	0.04
E14.5	Atoh1-EGFP	Dll1-mCherry	LDN 50nM	LSM780	41h30m	10	30	41.91	1.445	0.09	0.02
E14.5	Atoh1-EGFP	-	LDN 50nM	LSM780	44h50m	10	30	41.89	1.444	-	0.018
E14.5	Atoh1-EGFP	-	LDN 50nM	LSM880	53h50m	10	38	44.4	1.200	-	0.018
Average					**29h33m**	**6.5**	**26.3**	**39.92**	**1.589**	**0.07**	**0.098**

Movies

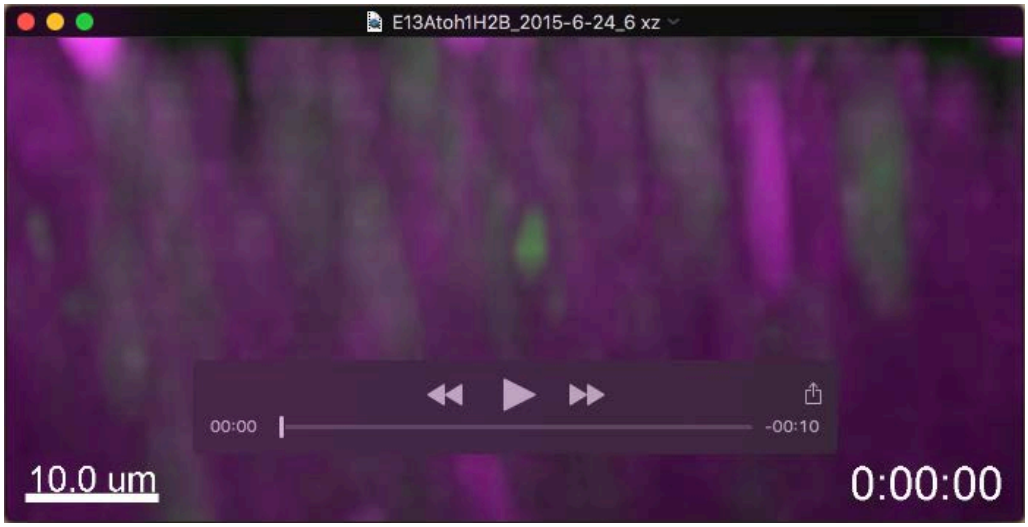

Movie 1

The view shown in **Fig. 3B-G**, containing xz projection images of the time-lapse experiment. The area of the x, y and z direction is 76.1 µm, 38.7 µm and 64.6 µm, respectively.

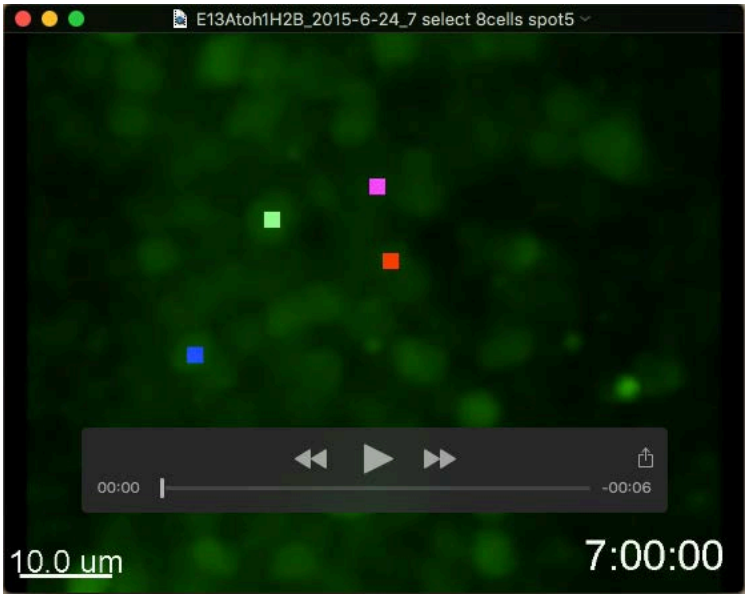

Movie 2

xy projection images of the time-lapse experiment using E13.5 *Atoh1*-EGFP;R26-H2B-mCherry cochlear explants between 7 and 19 h. Each color indicates cells 1–8, and is the same as in **Fig. 3L**.

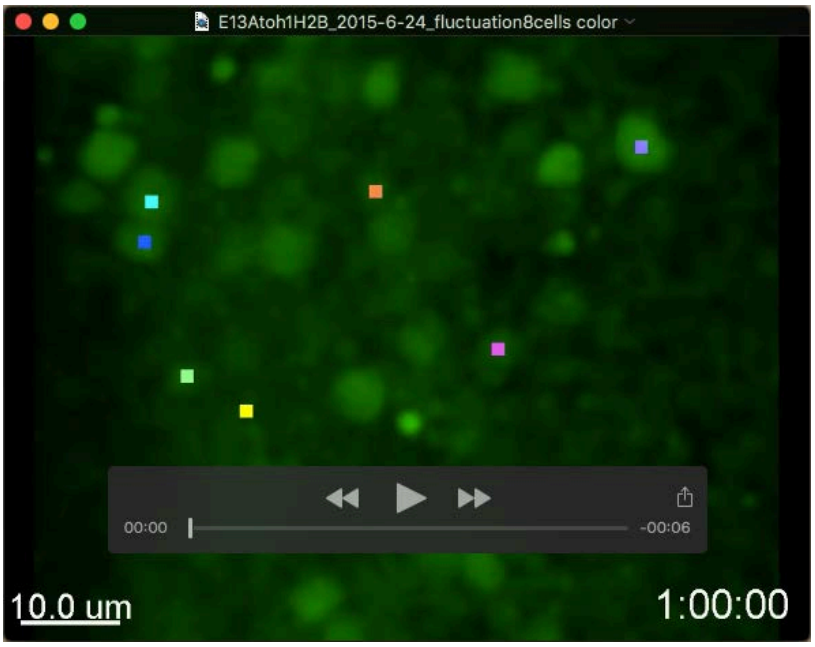

Movie 3

xy projection images of the time-lapse experiment using E13.5 *Atoh1*-EGFP;R26-H2B-mCherry cochlear explant**s** between 1 and 13 h. Each color of the points indicates cell**s** 9–16 and is the same as in **Fig. 3P**.

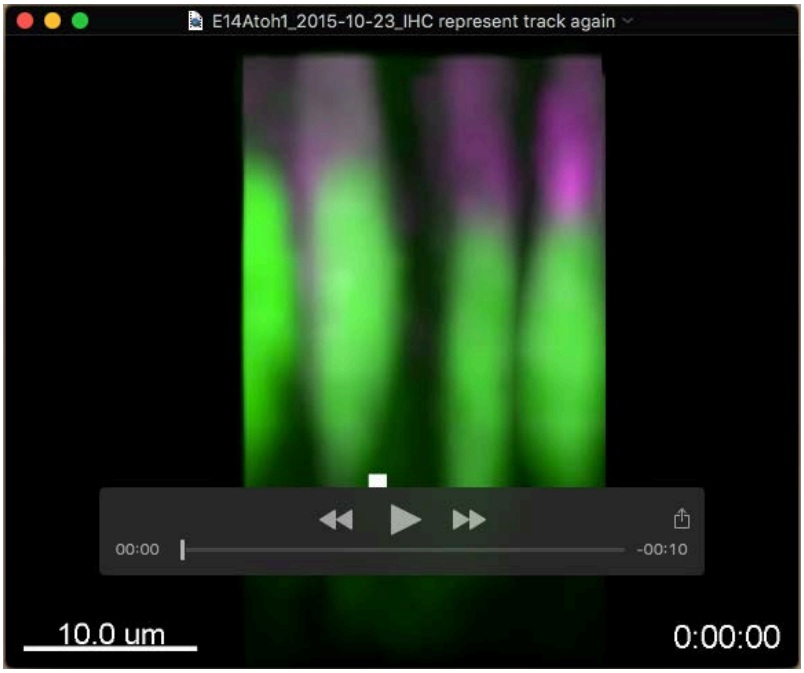

Movie 4

Two-dimensional yz projection images viewed from the medial side (the orientations are denoted by arrows between **Fig. 4A and 4A'**), focusing on presumptive IHCs indicated by white dots.

The depth of the x direction is 18.8 μm

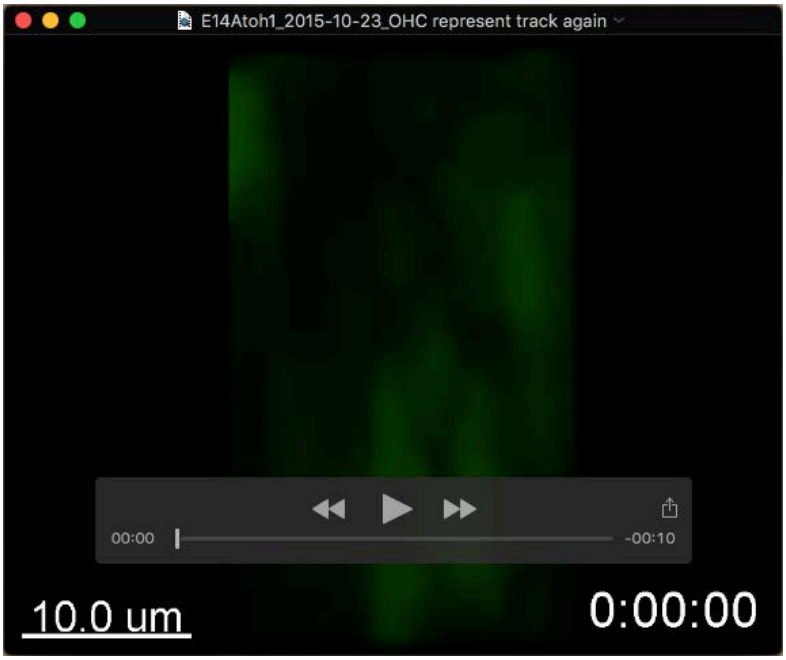

Movie 5

Two-dimensional yz projection images viewed from the lateral side (the orientations are denoted by arrows between **Fig. 4A and 4A'**), focusing on presumptive OHCs indicated by cyan dots.
The depth of the x direction is 26.3 μm

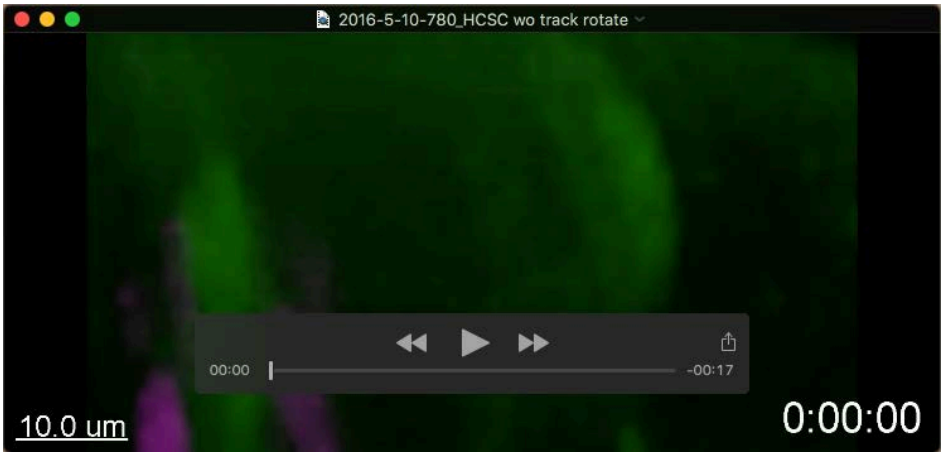

Movie 6

Two-dimensional xz projection images from 0 to 18 h; the image contrast of the GFP intensity was reduced twice, at 6 h and 12 h (**Supplemental Fig. 4F**). The depth of the y direction is 46.1 μm.

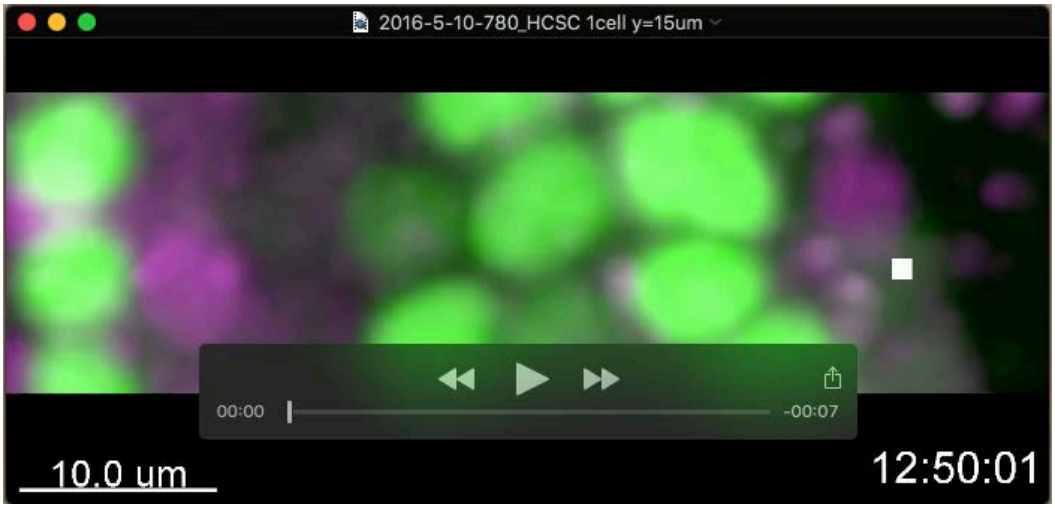

Movie 7

xy projection images of a representative neutral cell, which corresponds to the arrows in **Supplemental Fig. 4H**. The marked cell is adjacent to a high GFP and high-mCherry cell and moves up and down in Movie 8. The depth of the z direction is 41.8 μm.

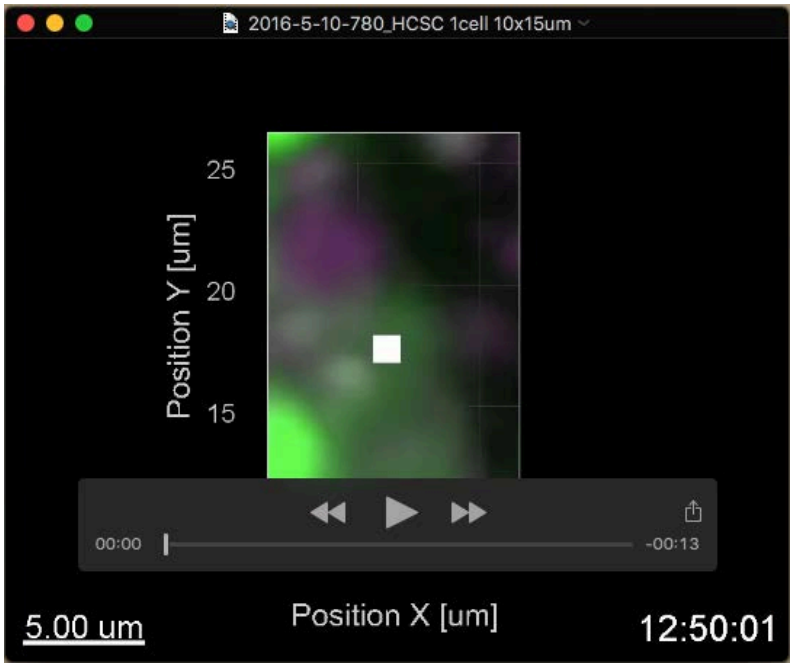

Movie 8

A magnified image of **Movie 7** containing a representative neutral cell, which corresponds to the arrows in **Supplemental Fig. 4O**. This movie is systematically rotated to maintain the marked cell in the foreground.

Movie 9

xy projection images of the time-lapse experiment using E14.5 *Atoh1*-EGFP cochlear explants. The snapshots of Movie 10 are shown in Fig.5D-N. Without color grouping.

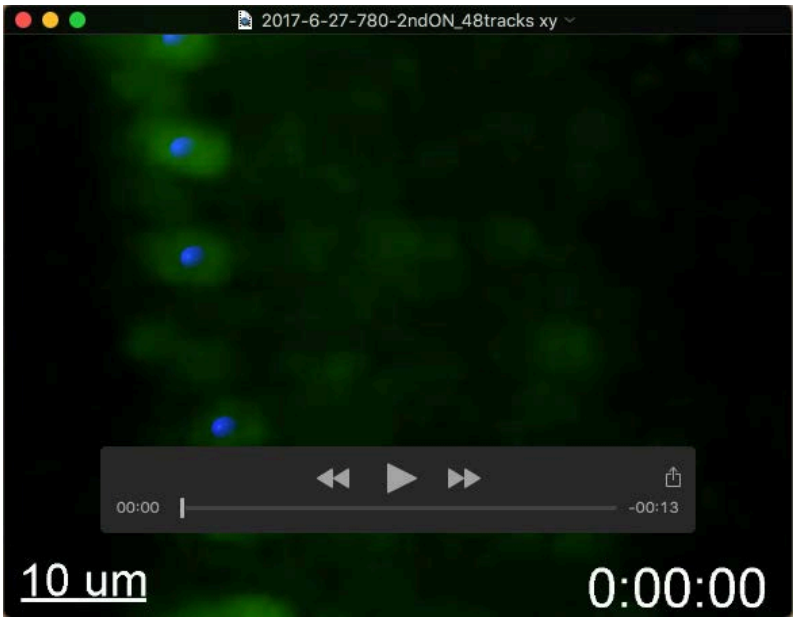

Movie 10

xy projection images of the time-lapse experiment using E14.5 *Atoh1*-EGFP cochlear explants. The snapshots of Movie 10 are shown in Fig.5D-N. With color grouping.

Movie 11

xz projection images of the time-lapse experiment using E14.5 *Atoh1*-EGFP cochlear explants. The snapshots of Movie 12 are shown in Fig. 5D'-N'. Without color grouping.

Movie 12

xz projection images of the time-lapse experiment using E14.5 *Atoh1*-EGFP cochlear explants. The snapshots of Movie 12 are shown in Fig. 5D'-N'. With color grouping.

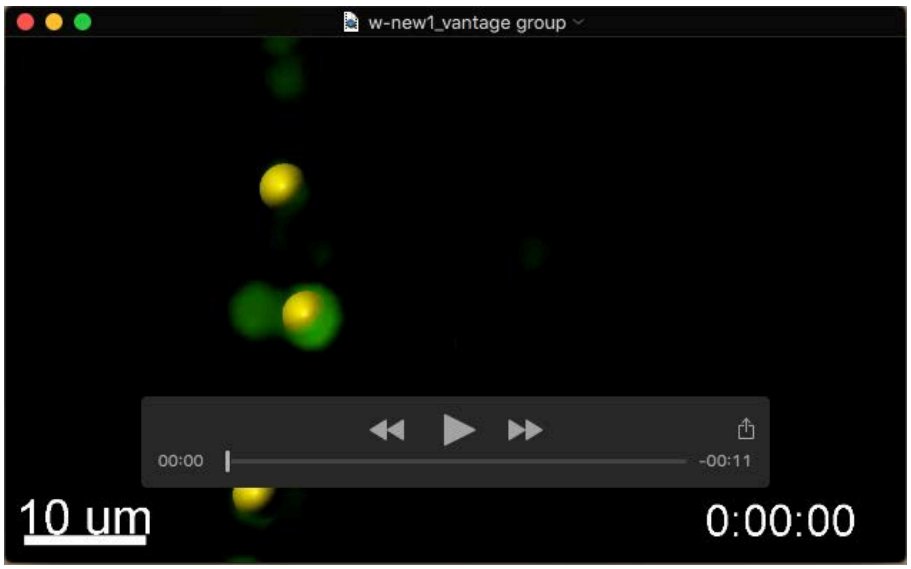

Movie 13

xy projection images of the time-lapse experiment using E14.5 *Atoh1*-EGFP cochlear explants, which corresponds to Fig. S6A, D, G.

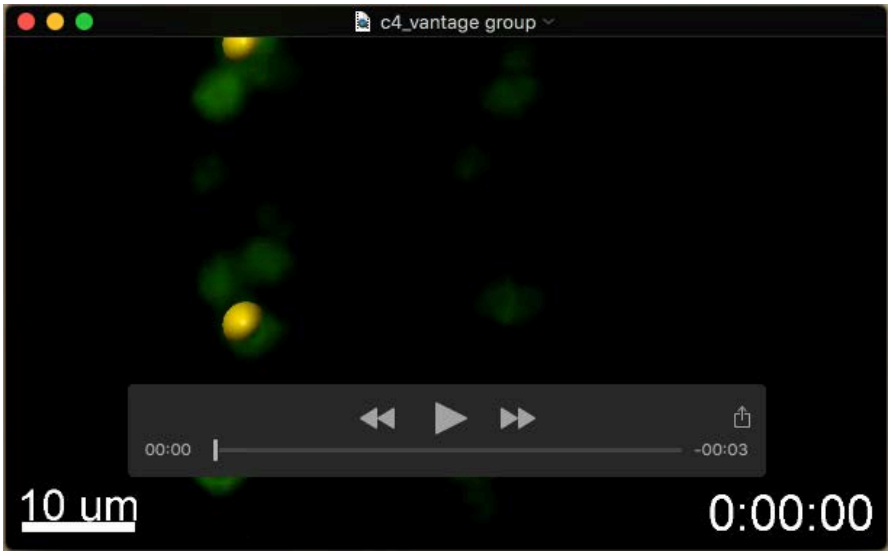

Movie 14

xy projection images of the time-lapse experiment using E14.5 *Atoh1*-EGFP cochlear explants with cyclopamine, which corresponds to Fig. S6B, E, H.

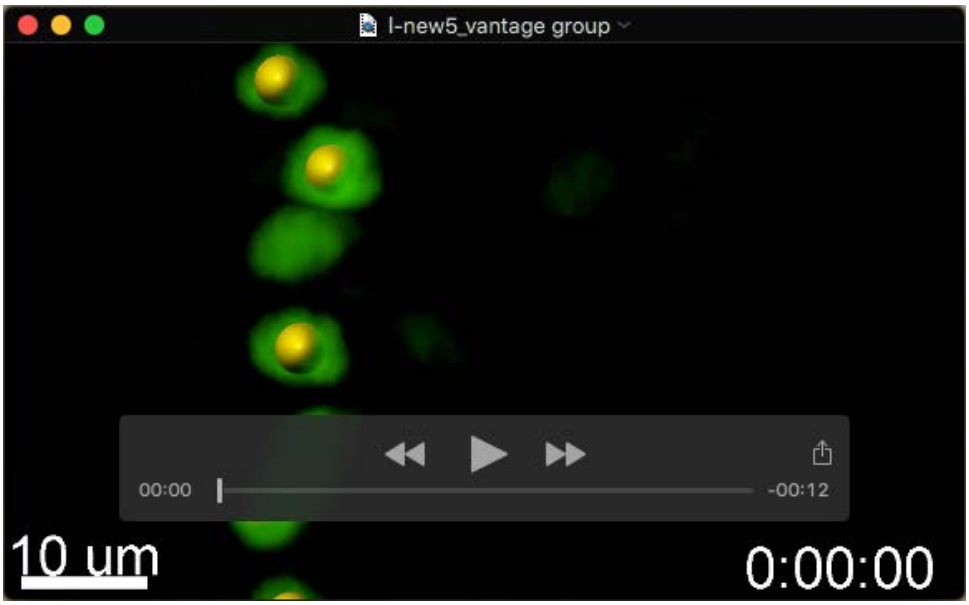

Movie 15

xy projection images of the time-lapse experiment using E14.5 *Atoh1*-EGFP cochlear explants with LDN193189, which corresponds to Fig. S6C, F, I.